

*Annual Review of Materials Research*

# Hybrid Improper Ferroelectricity: A Theoretical, Computational, and Synthetic Perspective

Nicole A. Benedek<sup>1</sup> and Michael A. Hayward<sup>2</sup>

<sup>1</sup>Department of Materials Science and Engineering, Cornell University, Ithaca, New York, USA;  
email: nbenedek@cornell.edu

<sup>2</sup>Department of Chemistry, University of Oxford, Oxford, United Kingdom;  
email: michael.hayward@chem.ox.ac.uk

Annu. Rev. Mater. Res. 2022. 52:331–55

The *Annual Review of Materials Research* is online at  
matsci.annualreviews.org

<https://doi.org/10.1146/annurev-matsci-080819-010313>

Copyright © 2022 by Annual Reviews.  
All rights reserved

ANNUAL  
REVIEWS **CONNECT**

[www.annualreviews.org](http://www.annualreviews.org)

- Download figures
- Navigate cited references
- Keyword search
- Explore related articles
- Share via email or social media

## Keywords

ferroelectricity, complex oxides, layered perovskites, first-principles calculations, synthesis

## Abstract

We review the theoretical, computational, and synthetic literature on hybrid improper ferroelectricity in layered perovskite oxides. Different ferroelectric mechanisms are described and compared, and their elucidation using theory and first-principles calculations is discussed. We also highlight the connections between crystal chemistry and the physical mechanisms of ferroelectricity. The experimental literature on hybrid improper ferroelectrics is surveyed, with a particular emphasis on cation-ordered double perovskites, Ruddlesden–Popper and Dion–Jacobson phases. We discuss preparative routes for synthesizing hybrid improper ferroelectrics in all three families and the conditions under which different phases can be stabilized. Finally, we survey some synthetic opportunities for expanding the family of hybrid improper ferroelectrics.

## 1. INTRODUCTION

The past two decades have been an exciting time for polar and ferroelectric materials. Advances in theory, first-principles computational techniques, and materials synthesis converged to produce new insights into mechanisms; illuminate the relationships among crystal structure, materials composition, and ferroelectric properties; and suggest new technological applications. In particular, building on the earlier work of Petzelt & Dvořák (1), Tagantsev and colleagues (2–4), Levanyuk & Sannikov (5), and others (6–9), synergistic theoretical, computational, and experimental efforts on perovskites and perovskite-related oxides have uncovered new pathways to ferroelectricity and polar structures involving nonpolar structural distortions. So-called hybrid improper or trilinearly coupled ferroelectrics (10–12) have greatly expanded the family of polar and ferroelectric perovskites. Whereas the twenty-first century began with only a handful of known polar and ferroelectric perovskites (perhaps most notably  $\text{BaTiO}_3$  and  $\text{PbTiO}_3$ ), we now have many examples of such materials, and most importantly, we also have a set of materials designs and structure–property relationships for finding more (13–21).

In this review, we survey some key families of experimentally synthesized hybrid improper ferroelectric layered perovskite oxides. Important differences among proper, improper, and hybrid improper ferroelectric mechanisms are clarified and some points of confusion that have arisen in the recent literature are addressed. We describe the chemical constraints to obtaining hybrid improper ferroelectricity in cation-ordered perovskites, Ruddlesden–Popper oxides, and Dion–Jacobson phases. There are only a limited number of thermodynamically stable layered perovskites that exhibit hybrid improper ferroelectricity due to the size and charge requirements of the metal cations. However, preparation of metastable phases via cation exchange offers the prospect of expanding the number and chemical range of hybrid improper ferroelectric oxides.

## 2. BRIEF OVERVIEW OF FERROELECTRIC MECHANISMS

### 2.1. Proper and Improper Ferroelectrics

Perhaps one of the most useful and successful approaches for exploring and understanding the physical characteristics of ferroelectrics, and structural phase transitions more generally, is the Landau theory of phase transitions (22). Landau theory describes structural phase transitions that occur between structures that adopt different space groups, between which there is a group–subgroup relation. This means that all of the symmetry elements of the low-symmetry phase are present in the high-symmetry phase. Landau theory is a phenomenological theory, meaning that “it relates measurable quantities to one another using a minimum set of input parameters” (23, p. 69). The input parameters can either be obtained from experiments or be calculated using first-principles (for example, density-functional theory) approaches. The goal is to obtain mathematically simple expressions that describe the experimentally observed phenomenon.

At the heart of Landau theory is the concept of the order parameter, which accounts for or represents the symmetry change that accompanies the transition. The order parameter is a physical feature or property of the system that breaks a particular symmetry of the high-symmetry phase. Either the order parameter itself or its derivatives (susceptibilities) can be measured experimentally and serve as the input parameters to a Landau theory. Some examples should help to illustrate these ideas.

The perovskite  $\text{BaTiO}_3$  belongs to the cubic  $Pm\bar{3}m$  space group at high temperatures and undergoes a phase transition to a tetragonal phase characterized by polar  $P4mm$  symmetry at around 398 K ( $\text{BaTiO}_3$  subsequently undergoes additional structural phase transitions, but we focus here on this first one). The transition is accompanied by the appearance of a spontaneous polarization, which we take to be the order parameter; it is zero in the cubic phase (since the  $Pm\bar{3}m$

space group contains the inversion as a symmetry operation) and increases to some finite value in the tetragonal phase. Hence, the order parameter breaks the inversion symmetry of the cubic phase and all other symmetries that would prevent the appearance of a macroscopic polarization. We note, however, that the order parameter does not contain any microscopic information; that is, it does not tell us what is giving rise to the polarization in terms of changes in bonding or the displacements of atoms. We return to this point below.

The free energy  $\mathcal{F}$  of the paraelectric cubic phase of BaTiO<sub>3</sub> can be expanded in powers of the order parameter, the polarization  $Q_P$  (for simplicity, we consider only a 1D order parameter), in the vicinity of the phase transition,

$$\mathcal{F} = \mathcal{F}_0 + \frac{1}{2}\alpha Q_P^2 + \frac{1}{4}\beta Q_P^4 + \frac{1}{6}\gamma Q_P^6, \quad 1.$$

where  $\mathcal{F}_0$  is the free energy when the polarization is zero and  $\alpha$ ,  $\beta$ , and  $\gamma$  are coefficients that we discuss in more detail below. The only terms that are allowed in the expansion, sometimes called invariants, are those that are compatible with the crystal symmetries of the given material. In this case, only even terms are allowed (only terms up to the sixth order are shown in Equation 1), and the reason can be understood intuitively. An applied electric field switches the direction, or sign, of the polarization in a ferroelectric, but the overall space group does not change. Hence, both the up and down phases of the material are identical and therefore must have the same free energy. If the sign of  $Q_P$  changes in Equation 1, only even-order terms will allow  $\mathcal{F}$  to remain invariant. Note that Equation 1 is general and applies to any proper ferroelectric; it is not specific to BaTiO<sub>3</sub>. Indeed, one of the great strengths of Landau theory is its universality.

What about the coefficients in these equations? As **Figure 1** shows, the coefficient  $\alpha$  is temperature dependent and defines the curvature of the free energy about the polarization minimum; it is positive in the paraelectric phase above the phase transition, close to zero at or near the phase transition, and negative in the paraelectric phase below the transition temperature (the properties of the paraelectric phase can be studied below the transition temperature using first-principles calculations, as described below). The coefficient  $\beta$  does not depend on temperature, but its sign

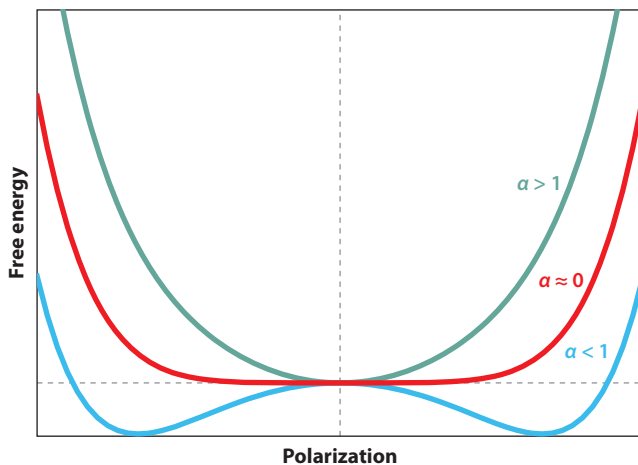


**Figure 1**

Schematic illustration of the behavior of the free energy of a proper ferroelectric as a function of the polarization. The variable  $\alpha$  appears in the free energy expansion of the paraelectric phase,

$$\mathcal{F} = \mathcal{F}_0 + \frac{1}{2}\alpha Q_P^2 + \frac{1}{4}\beta Q_P^4 + \frac{1}{6}\gamma Q_P^6.$$

indicates the nature of the phase transition, either continuous ( $\beta > 0$ ) or discontinuous ( $\beta < 0$ ). The coefficient  $\gamma$  must be positive in a stable material (23).

Atomic displacements are not the only changes that occur during the phase transition. The unit cell also changes size and shape—in other words, the phase transition is also accompanied by a spontaneous strain, which can be considered as an additional order parameter.<sup>1</sup> The free energy then contains additional terms that show how the polarization and strain are coupled,

$$\mathcal{F} = \mathcal{F}_0 + \frac{1}{2}\alpha Q_p^2 + \frac{1}{4}\beta Q_p^4 + \frac{1}{2}\alpha_\epsilon Q_\epsilon^2 + \frac{1}{4}\beta_\epsilon Q_\epsilon^4 + \gamma Q_\epsilon Q_p^2, \quad 2.$$

where  $Q_\epsilon$  represents the strain and the Greek letters are again coefficients. Which feature—the polarization or the strain—is the primary order parameter? If only the strain is considered while the atoms are fixed in their high-symmetry positions, then the symmetry is reduced from  $Pm\bar{3}m$  to  $P4/mmm$ . This is higher than the experimentally observed space group in the tetragonal ferroelectric phase. However, if the atoms are displaced without first deforming the unit cell, then the symmetry is reduced to  $P4mm$ . Hence, the polarization induced by the atomic displacements is the primary order parameter, and the strain, a secondary order parameter, is merely coupled to the polarization and becomes nonzero only in the presence of the polarization. This manifests mathematically in Equation 2 as a linear coupling of the strain to the polarization,  $Q_\epsilon Q_p^2$ . Ferroelectric phase transitions in which the polarization is the primary order parameter are classified as proper. Hence, BaTiO<sub>3</sub> is a proper ferroelectric and an improper ferroelastic.

Where does the polarization come from at a microscopic level? First-principles calculations have delivered a wealth of insights into this question for BaTiO<sub>3</sub> and also many other systems (14, 24, 25). In the specific case of BaTiO<sub>3</sub>, the polarization arises from a so-called soft mode (26, 27) associated with displacements of the barium and titanium atoms against the oxygen atoms. This mode transforms like the irreducible representation  $\Gamma_4^-$  of the  $Pm\bar{3}m$  space group and results in changes in the bonding between (primarily) the titanium and oxygen atoms. In first-principles calculations of the cubic phase, which are almost always performed at 0 K, this soft mode has a negative force constant.<sup>2</sup> This indicates that the cubic phase is not the most stable phase at low temperatures. A plot of energy versus soft mode displacement would produce the  $\alpha < 1$  curve in **Figure 1**; the cubic phase would be located at the saddle point (zero soft mode displacement), and the two minima correspond to the two different directions of the polarization in the lower-energy  $P4mm$  phase.

Not all ferroelectrics undergo proper ferroelectric phase transitions. A large number of ferroelectrics undergo phase transitions in which the polarization is a secondary order parameter, and these are known as improper ferroelectrics (5). Perhaps the canonical example of this class of materials is YMnO<sub>3</sub>, a multiferroic hexagonal (not perovskite) manganite. The phase transition mechanism in YMnO<sub>3</sub> was debated for many years but was finally elucidated with the help of first-principles calculations (28, 29). The transition from the high-temperature paraelectric  $P6_3/mmc$  phase to the ferroelectric  $P6_3cm$  ground state is accompanied by a tripling of the primitive unit cell volume (a so-called zone-tripling transition). Fennie & Rabe (29) showed that the primary order parameter is a zone-boundary phonon mode of the  $P6_3/mmc$  phase that transforms like the irreducible representation  $K_3$ . This mode buckles the MnO<sub>3</sub> layer (which arises from the apex-linked sheet of MnO<sub>5</sub> trigonal bipyramids) and induces a small ( $\approx 0.1 \mu\text{C}/\text{cm}^2$ ) polarization. The

<sup>1</sup>Materials that exhibit a spontaneous strain are termed ferroelastic.

<sup>2</sup>The force constant is proportional to the square of the phonon frequency, with negative force constants leading to imaginary phonon frequencies. In many theoretical studies, an imaginary phonon frequency, rather than a negative force constant, is reported for soft ferroelectric modes.

majority of the polarization, experimentally observed to be around  $5 \mu\text{C}/\text{cm}^2$  (30), arises from the coupling between the  $K_3$  mode and a zone-center mode that transforms like  $\Gamma_2^-$  and results in a buckling of the yttrium planes. Note that the  $\Gamma_2^-$  mode by itself does not enlarge the unit cell and therefore cannot account for the experimentally observed tripling of the unit cell volume. In addition, first-principles calculations showed that the  $\Gamma_2^-$  mode becomes energetically favorable only in the presence of the  $K_3$  mode; that is, by itself, it raises the energy of the  $P6_3/mmc$  phase. Hence,  $\text{YMnO}_3$  undergoes an improper ferroelectric phase transition in which the primary order parameter is a structural distortion with  $K_3$  symmetry. The polarization, with  $\Gamma_2^-$  symmetry, is a secondary order parameter that is coupled to the  $K_3$  mode.

The free energy of the paraelectric  $P6_3/mmc$  phase of  $\text{YMnO}_3$  can be expanded in powers of the order parameters in the same manner as we showed above for  $\text{BaTiO}_3$ . However, given the improper nature of the phase transition, the form of the free energy is rather different than that for a proper ferroelectric,

$$\mathcal{F} = \mathcal{F}_0 + \alpha_{20} Q_{K_3}^2 + \alpha_{02} Q_P^2 + \beta_{40} Q_{K_3}^4 + \beta_{04} Q_P^4 + \beta_{31} Q_{K_3}^3 Q_P + \beta_{22} Q_{K_3}^2 Q_P^2, \quad 3.$$

where  $Q_{K_3}$  is the amplitude of the  $K_3$  mode using the notation from Reference 29 (see Reference 31 for the general form of the polarization order parameter). The last term of Equation 3, the biquadratic term, is allowed by symmetry even in proper ferroelectrics with multiple order parameters. It is the cubic (in  $K_3$ ) term,  $\beta_{31} Q_{K_3}^3 Q_P$ , that distinguishes  $\text{YMnO}_3$  as an improper ferroelectric. Note that the polarization, the secondary order parameter, is coupled linearly to the primary order parameter, the  $K_3$  mode. This is exactly analogous to the case of improper ferroelasticity in  $\text{BaTiO}_3$  discussed earlier, where the strain, the secondary order parameter, is coupled linearly to the primary order parameter, the polarization, in Equation 2. As **Figure 2** shows, the behavior of the polarization in  $\text{YMnO}_3$  about the paraelectric phase is quite different from that of a proper ferroelectric like  $\text{BaTiO}_3$ . In particular, the polarization remains in a single well potential, and the minimum merely shifts to finite values as the  $K_3$  mode switches on. Since the polarization is coupled to the  $K_3$  mode, it will only switch when the  $K_3$  mode switches.

It is important to understand what **Figure 2** is illustrating because such plots can be misread. Specifically, we state above that the two wells of the double well potential in **Figure 1** represent the

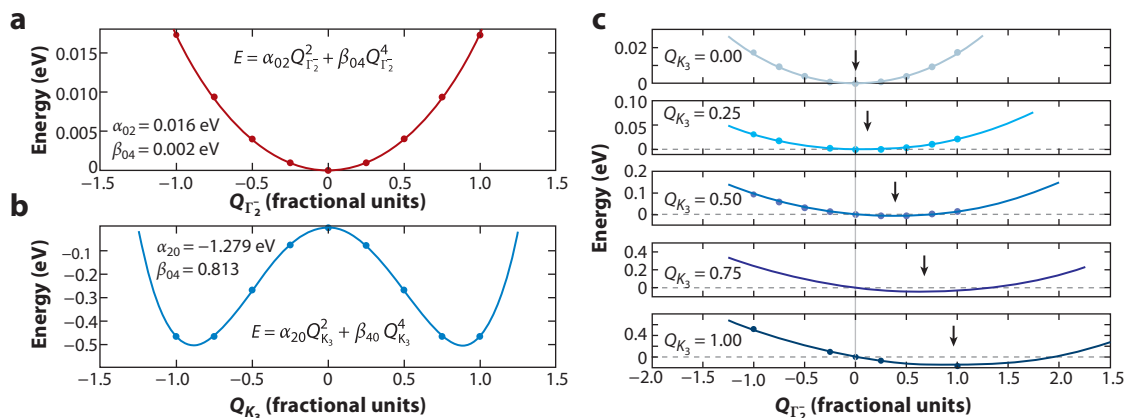


**Figure 2**

Energy of  $\text{YMnO}_3$  as a function of the amplitude of (a) the polarization by itself ( $\Gamma_2^-$  mode) and (b) the  $K_3$  mode by itself. (c) Energy of  $\text{YMnO}_3$  in the ferroelectric phase as a function of the amplitude of the polarization ( $\Gamma_2^-$  mode) for a series of fixed amplitudes of the  $K_3$  mode from first-principles calculations. Note that  $Q_{K_3} = 1$  denotes the full amplitude of the  $K_3$  mode of fully relaxed  $\text{YMnO}_3$ .

Figure adapted with permission from Reference 29; copyright 2005 American Physical Society.

two different directions of polarization that can be switched between with an applied electric field. Hence, one may interpret **Figure 2** as suggesting that the polarization in  $\text{YMnO}_3$  is not switchable since the polarization appears only as a single well, but this is not the case—the polarization in  $\text{YMnO}_3$  is indeed switchable, as it must be in any true ferroelectric. The key is to realize that **Figure 2** conveys information only about the ferroelectric mechanism and not the polarization switching pathway.<sup>3</sup> **Figure 2b** shows one direction of the polarization; the other direction would appear as a single well with an identical energy minimum except at  $Q_{\Gamma_2^-} = -1$  (the  $K_3$  mode would also switch sign since the two distortions are coupled, as mentioned above). Only the primary order parameter, in this case the  $K_3$  mode, is required to exhibit a double well potential, and it does, as **Figure 2b** shows.

**Figure 2** makes clear that the origin of the polarization in an improper ferroelectric,  $\text{YMnO}_3$  in this case, is different from that of proper ferroelectric. These details directly affect experimental observations (and their interpretation) of ferroelectricity and the ferroelectric phase transition in  $\text{YMnO}_3$ . For example, **Figure 2** suggests that a direct transition from  $P6_3/mmc$  into the ferroelectric  $P6_3mc$  phase is unlikely, because in the absence of the  $K_3$  mode ( $Q_{K_3} = 0$ ), the  $\Gamma_2^-$  mode that would drive such a transition is stable and raises the energy of the paraelectric phase.

Connecting the physical mechanisms of ferroelectric phase transitions to changes in bonding and crystal chemistry is an extremely powerful approach to the discovery of polar and ferroelectric materials. The physical mechanism of improper ferroelectricity differs from that of proper ferroelectricity, and the crystal chemical driving forces also differ between the two mechanisms. In the case of the proper ferroelectric  $\text{BaTiO}_3$ , the pioneering calculations of Cohen (24) [and subsequent work by many others (e.g., 14)] showed that the ferroelectric distortion leads to significant hybridization between the 3d states on titanium and the 2p states of oxygen. In fact, if this Ti–O interaction is artificially suppressed, then the ferroelectric distortion is as well, and the cubic  $Pm\bar{3}m$  phase is stable (24). This mechanism can also be described as a second-order Jahn–Teller (SOJT) effect in the framework of vibronic coupling theory (33).

Hybridization between the titanium 3d and oxygen 2p states is also essential to the ferroelectric distortion of  $\text{PbTiO}_3$ , but here there are additional factors at play. The lead atom is formally in a 2+ oxidation state, and therefore, the outer shell electron configuration is  $6s^2 6p^0$ . Extensive prior studies of oxides containing cations with  $ns^2 np^0$  configurations have shown that there is a strong interaction between the 2p orbitals of oxygen and the ns and np orbitals of the cation (34–36). Specifically, in such compounds there is an antibonding cation ns–O 2p interaction at the top of the valence band. Since these states are filled, the interaction is energetically destabilizing. A reduction in the symmetry of the cation site (via a ferroelectric distortion, for example) allows some unfilled cation np orbitals to mix with the cation ns–O 2p states to produce a localized nonbonding state, often referred to as a lone pair, at the top of the valence band. The presence of the filled 6s orbital on lead in  $\text{PbTiO}_3$  produces a large strain that accompanies the displacements of ions from their centrosymmetric positions in the cubic phase. This strain stabilizes a tetragonal  $P4mm$  ground state for  $\text{PbTiO}_3$  in contrast to the rhombohedral  $R3m$  space group adopted by  $\text{BaTiO}_3$  at temperatures below about 200 K (24). The presence of the filled 6s orbital on the  $\text{Bi}^{3+}$  cation has also been shown to be responsible for the ferroelectric distortion in bismuth-containing perovskites, such as  $\text{BiFeO}_3$  (37, 38). However, the presence of a  $\text{Bi}^{3+}$  cation, or an  $ns^2 np^0$  electron configuration in general, does not guarantee a polar distortion (39).

The crystal chemical origin of the most extensively studied improper ferroelectrics, the hexagonal manganites, differs from that of the proper ferroelectrics discussed above. Specifically,

<sup>3</sup> Polarization switching in ferroelectrics can be complex (see References 31 and 32 for a discussion of switching in multiferroic hexagonal manganites).

Van Aken and coworkers (28) used first-principles calculations to show that, in contrast to the perovskite titanates, the Born effective charges of the yttrium, manganese, and oxygen ions in  $\text{YMnO}_3$  are close to the nominal ionic charges of these species. The Born effective charge is defined as the change in macroscopic polarization with respect to an atomic displacement at zero electric field (40, 41). In simple terms, one can think of the Born effective charge as an indicator of “a change in covalency during ionic displacement” (42, p. 8). The Born effective charge of the titanium atom in  $\text{BaTiO}_3$  is around +7, much larger than the +4 nominal ionic charge of titanium in this compound. This anomalously large charge indicates that there is a significant change in titanium 3d–oxygen 2p hybridization upon a small displacement of the titanium atoms (the Born effective charge of the oxygen atoms in  $\text{BaTiO}_3$  is similarly anomalous, around  $-5$  in the direction of the Ti–O bonds). Inspecting the Born effective charges of  $\text{YMnO}_3$ , along with an analysis of the density of states in the paraelectric and ferroelectric phases, allowed Van Aken et al. to conclude that the ferroelectric phase transition in  $\text{YMnO}_3$  is associated with very little rehybridization. Instead, the transition is driven by ionic size effects related to the small  $\text{Y}^{3+}$  cations and large  $\text{MnO}_5$  polyhedra, which result in tilting of the  $\text{MnO}_5$  bipyramids and large Y–O displacements. Such materials are known as geometric ferroelectrics. Subsequent work suggests that  $\text{BaNiF}_4$  (43) and the fluoroperovskites (44) are also geometric ferroelectrics.

## 2.2. Hybrid Improper Ferroelectrics

The past decade has witnessed significant progress on an additional class of ferroelectrics, so-called hybrid improper ferroelectrics. In these materials, there exists a term in the free energy,  $Q_P Q_{R1} Q_{R2}$ , in which the polarization is trilinearly coupled to two other nonpolar structural distortions, where  $Q_{R1}$  and  $Q_{R2}$  are the amplitudes of the nonpolar modes. The concept of hybrid improper ferroelectricity was introduced in Reference 12 as a mechanism to enable electric field switching of the magnetization in multiferroic materials. However, the possibility and potential importance of a trilinear coupling between different order parameters in polar materials were previously recognized in References 9 and 10. **Table 1** lists a number of experimentally synthesized layered perovskites in which a polar structure is known to emerge via a hybrid improper mechanism.

The Ruddlesden–Popper phases  $\text{Ca}_3\text{Ti}_2\text{O}_7$  and  $\text{Ca}_3\text{Mn}_2\text{O}_7$  were identified as hybrid improper ferroelectrics in Reference 12. The origin of the polar structures of these materials was something of a mystery because neither of their parent perovskites,  $\text{CaTiO}_3$  and  $\text{CaMnO}_3$ , is polar (like most perovskites, both materials instead crystallize in the nonpolar  $Pnma$  space group).  $\text{Ca}_3\text{Ti}_2\text{O}_7$  and  $\text{Ca}_3\text{Mn}_2\text{O}_7$  both adopt tetragonal  $I4/mmm$  symmetry at high temperatures and undergo structural phase transitions to the polar space group  $A2_1am$ . Group theoretical analysis (12) showed that this polar phase is related to the nonpolar tetragonal phase by three distinct structural distortions: a zone-center polar mode transforming like the irreducible representation (irrep)  $\Gamma_5^-$  and two zone-boundary nonpolar modes corresponding to rotations of the  $\text{BO}_6$  octahedra transforming like the irreps  $X_2^+$  and  $X_3^-$ . The free energy expansion about the tetragonal phase that involves all three modes is then given by

$$\begin{aligned} \mathcal{F} = & \mathcal{F}_0 + \alpha_{200} Q_P^2 + \alpha_{020} Q_{X_2^+}^2 + \alpha_{002} Q_{X_3^-}^2 + \beta_{400} Q_P^4 + \beta_{040} Q_{X_2^+}^4 + \beta_{004} Q_{X_3^-}^4 \\ & + \gamma_{220} Q_P^2 Q_{X_2^+}^2 + \gamma_{202} Q_P^2 Q_{X_3^-}^2 + \gamma_{022} Q_{X_2^+} Q_{X_3^-} + \delta Q_P Q_{X_2^+} Q_{X_3^-}, \end{aligned} \quad 4.$$

where  $Q_P$  is the amplitude of the  $\Gamma_5^-$  mode. The  $\Gamma_5^-$  mode can break the inversion symmetry of the  $I4/mmm$  phase to produce a macroscopic polarization. However, it does not produce a structure

**Table 1** Experimentally synthesized layered perovskite and perovskite-like crystals in which a polar structure emerges through a hybrid improper or trilinear coupling mechanism

Material	Reference(s)
<b>Cation-ordered perovskites</b>	
$\text{NaLnMnWO}_6$ ( $Ln = \text{La, Nd, Tb, Y}$ )	45–48
$\text{NaLnFeWO}_6$ ( $Ln = \text{La, Nd, Pr, Sm}$ )	49, 50
$\text{NaLnCoWO}_6$ ( $Ln = \text{Sm–Er, Y, Yb}$ )	51, 52
$\text{NaLnNiWO}_6$ ( $Ln = \text{La–Tb, Y, Dy, Ho, Yb}$ )	53, 54
<b><math>n = 2</math> Aurivillius phases</b>	
$\text{SrBi}_2\text{Nb}_2\text{O}_7$	55
$\text{SrBi}_2\text{Ta}_2\text{O}_7$	56, 57
<b><math>n = 2</math> Ruddlesden–Popper phases</b>	
$\text{Ca}_3\text{Mn}_2\text{O}_7$	58
$\text{Ca}_3\text{Ti}_2\text{O}_7$	58
$(\text{Ca, Sr})_3\text{Ti}_2\text{O}_7$	59
$\text{Sr}_3\text{Zr}_2\text{O}_7$	60
$(\text{Ca, Sr})_3\text{Sn}_2\text{O}_7$	61
$\text{Li}_2\text{AB}_2\text{O}_7$ ( $A = \text{Sr, Ca}; B = \text{Nb, Ta}$ )	62
$\text{LiNdB}_2\text{O}_7$ ( $B = \text{Nb, Ta}$ )	63
$(\text{Ca, Sr, Tb})_3(\text{Fe/Ti})_2\text{O}_7$	64
$\text{Li}_2\text{La}(\text{TaTi})\text{O}_7$	65
<b><math>n = 2</math> Dion–Jacobson phases</b>	
$\text{CsBiNb}_2\text{O}_7$	66
$\text{RbBiNb}_2\text{O}_7$	67
$\text{CsNdB}_2\text{O}_7$ ( $B = \text{Nb, Ta}$ )	66, 68, 69
$\text{RbNdB}_2\text{O}_7$ ( $B = \text{Nb, Ta}$ )	68, 69
$\text{CsLaNb}_2\text{O}_7$	70

with the experimentally observed  $A2_1am$  symmetry. Furthermore, in  $\text{Ca}_3\text{Mn}_2\text{O}_7$ , structural distortion modes with  $\Gamma_5^-$  symmetry raise the energy of the  $I4/mmm$  phase by themselves (they are so-called hard modes with real frequencies or positive force constants). The  $X_2^+$  and  $X_3^-$  modes can each individually lower the energy of the  $I4/mmm$  phase, but again, neither distortion produces a structure with  $A2_1am$  symmetry, and since they are nonpolar modes, they cannot break inversion symmetry by themselves. Instead, the  $X_2^+$  and  $X_3^-$  modes together establish the  $A2_1am$  symmetry of the  $\text{Ca}_3\text{Mn}_2\text{O}_7$  ground state ( $X_2^+ \oplus X_3^-$ ) and make up a hybrid primary order parameter that drives the transition to the ferroelectric phase. The  $\Gamma_5^-$  modes couple to the hybrid order parameter and enhance the macroscopic polarization but do not drive the phase transition themselves. As **Figure 3** shows, the behavior of the polar modes in  $\text{Ca}_3\text{Mn}_2\text{O}_7$  is very similar to that of the polar modes in the improper ferroelectric  $\text{YMnO}_3$ .

The form of the trilinear term means that when the polarization switches in such a material, either one of the two modes making up the hybrid order parameter will switch but not both. The question of how ferroelectric switching actually proceeds in such materials is complex, and it is generally not possible to deduce the lowest-energy switching pathways by simple inspection of the trilinear invariant. For example, in previous work (71), group theoretical analysis and first-principles calculations were used to show that polarization switching in  $\text{Ca}_3\text{Ti}_2\text{O}_7$  may proceed via one of several possible low-energy two-step pathways in which the order parameters rotate (change phase) at constant amplitude.

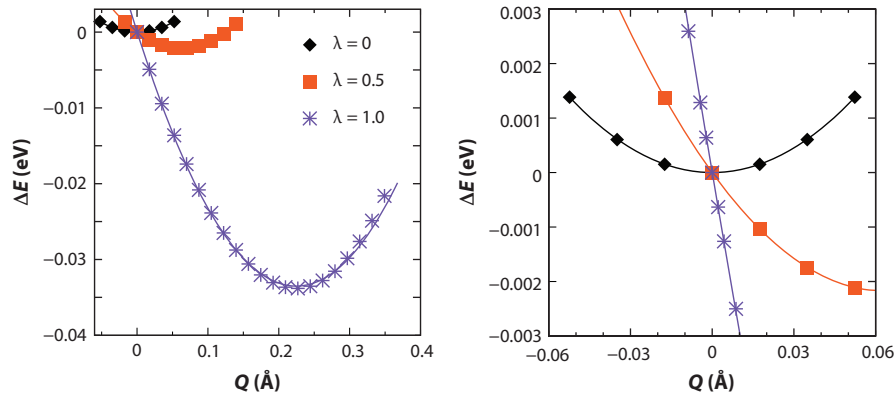


**Figure 3**

Change in the energy per formula unit of the paraelectric  $I4/mmm$  phase of  $\text{Ca}_3\text{Mn}_2\text{O}_7$  from first-principles calculations as a function of the amplitude of the polar  $\Gamma_5^-$  mode in the presence of a hybrid order parameter,  $Q_{X_{23}} = \lambda Q_{X_3^-} Q_{X_2^+}$ . A value of  $\lambda = 1$  denotes the amplitude of the hybrid order parameter in the fully relaxed  $A2_{1am}$  ground state. The right-hand image shows the region around  $\Delta E = 0$  at greater magnification (note the difference in scales between the left- and right-hand images). Figure adapted with permission from Reference 11.

The origin of the polarization—that is, which order parameter induces the polar ground state—can also be unclear in materials such as  $\text{Ca}_3\text{Ti}_2\text{O}_7$  that have unstable polar zone-center modes in addition to instabilities of the modes making up the hybrid order parameter. In these materials, there exists the possibility that a polar zone-center mode first drives a proper ferroelectric transition to an intermediate polar phase, followed by one or more subsequent structural phase transitions corresponding to the nonpolar modes making up the hybrid order parameter.<sup>4</sup> Indeed, in this sense the hybrid improper terminology is somewhat unfortunate because the designations of proper and improper generally refer to details of phase transitions. However, what is often of interest instead is the coupling between modes making up the hybrid order parameter with other modes and their connections to materials properties. It is very difficult to address issues related to phase transitions in materials involving multiple modes using symmetry arguments alone, although previous work (72) has suggested that it is possible to identify the key fingerprint of improper ferroelectricity from first-principles calculations. Specifically, in improper ferroelectrics there is a kink in the energy as a function of the macroscopic electric displacement field. Instead of the double well potential characteristic of proper ferroelectrics, improper ferroelectrics exhibit two separate single wells (one for each direction of the polarization), which cross at zero energy and zero displacement field, producing a discontinuity in the electrical equation of state. This feature identifies a material as an improper ferroelectric. Although the ability to compute properties as a function of a fixed displacement field is not available in all first-principles electronic structure codes, it is available in some of the most commonly used packages, and we believe this method is underutilized.

Finally, the presence of particular cations in a given material can also lead to confusion as to the origin of polar structures in hybrid improper ferroelectrics. Specifically, in materials

<sup>4</sup>An additional possibility is that one of the modes making up the hybrid order parameter first drives a structural phase transition to a nonpolar intermediate phase. The polar mode and the second nonpolar mode making up the hybrid order parameter then mix and drive the transition to the polar ground state. This would also be a proper ferroelectric transition, and such materials have been termed weakly polar ferroelectrics (3, 4).

containing SOJT-active cations (such as  $\text{Ti}^{4+}$  and  $\text{Nb}^{5+}$ ) at the octahedral site, it is often claimed that off-centering of the SOJT cation occurs via the SOJT mechanism (73) or that the SOJT mechanism is in competition with the hybrid improper mechanism. However, in many hybrid improper ferroelectrics, off-centering of SOJT cations has nothing whatsoever to do with the SOJT nature of the cation itself. In these materials, hybrid improper ferroelectricity persists even if the SOJT cation is replaced with a non-SOJT-active cation (this is most easily accomplished computationally using first-principles calculations, as done in Reference 74, for example). Off-centering of the SOJT cation occurs because the various (polar and nonpolar) modes that are involved in establishing the polar ground state break the symmetries that would otherwise keep this cation centered in the octahedron. While there may in fact be competition between SOJT-driven (proper) and hybrid improper ferroelectricity in a given material, as described below, this can be established only through careful investigation, not through simple inspection of the material composition.

The crystal chemical origins of hybrid improper ferroelectricity vary, depending on which modes drive the transition and on the material itself. However, hybrid improper ferroelectricity has been investigated most intensively in layered perovskites so far, and in these materials, modes involving tilts or rotations of the transition metal octahedra appear to play a major role in establishing the polar ground state. There have been extensive previous studies of these distortions in  $\text{ABO}_3$  perovskites, which chemical and physical forces drive them, and the relationship between composition and the particular tilt or rotation pattern adopted by a given perovskite (75–81). The rotation pattern perhaps most commonly observed in hybrid improper layered perovskites is that described as  $a^- a^- c^+$  in Glazer notation (75). This is the same rotation pattern exhibited by perovskites that crystallize in the  $Pnma$  space group, the most commonly adopted space group for perovskites. Prior work (80) has shown that, in this space group and rotation pattern,  $A$ –O covalent bonding is maximized and repulsive  $A$ –O interactions are minimized. The pattern is adopted when the  $A$ -site becomes relatively electronegative or when the tolerance factor falls below around 0.97. In  $Pnma$  perovskites that adopt the  $a^- a^- c^+$  rotation pattern, the  $A$ -site cations displace, leading to local dipoles within the  $A$ –O layers. However, the  $A$ -sites are related by inversion symmetry through the  $B$ -site, leading to layer dipoles in adjacent layers that are equal and oriented in opposite directions, as shown in **Figure 4a**, so there is zero macroscopic polarization.

In  $A_{n+1}B_n\text{O}_{3n+1}$  Ruddlesden–Popper phases,  $A'[A_{n-1}B_n\text{O}_{3n+1}]$  Dion–Jacobson phases,  $A$ -site ordered  $AA'B_2\text{O}_6$  double perovskites, and other layered systems, the  $B$ -site inversion symmetry of the constituent perovskite blocks is broken by cation ordering or other structural features (note that our discussion here refers to even- $n$  Ruddlesden–Popper and Dion–Jacobson phases; odd- $n$  phases may still be polar, but the mechanism may be different). In Ruddlesden–Popper phases and  $A$ -site ordered double perovskites, this allows a nonzero macroscopic polarization to arise through the noncancellation of layer dipoles, as shown in **Figure 4** (15, 17). At first sight, it may appear as if maximizing the magnitude of the layer dipoles is the best strategy to achieve a large overall macroscopic polarization. However, previous work (17) has shown that if the dipoles in different  $A$ –O layers are of similar magnitude (whether large or small), then they will almost completely cancel out, leading to a small macroscopic polarization. In order to maximize the polarization, the dipoles induced in the  $A$ –O layers should be as different in magnitude as possible. In  $AA'B_2\text{O}_6$  double perovskites and cation-ordered Ruddlesden–Popper phases, this guideline can be expressed as a simple crystal chemical design rule—the polarization is proportional to the difference in the tolerance factors of the parent perovskites. The  $A$ -site displacements that induce the layer polarizations are coupled to the rotations and tilts and are larger or smaller when the octahedral rotations are larger or smaller, respectively; in general, the smaller the tolerance factor for a given perovskite is, the larger the magnitude of the rotations and tilts.

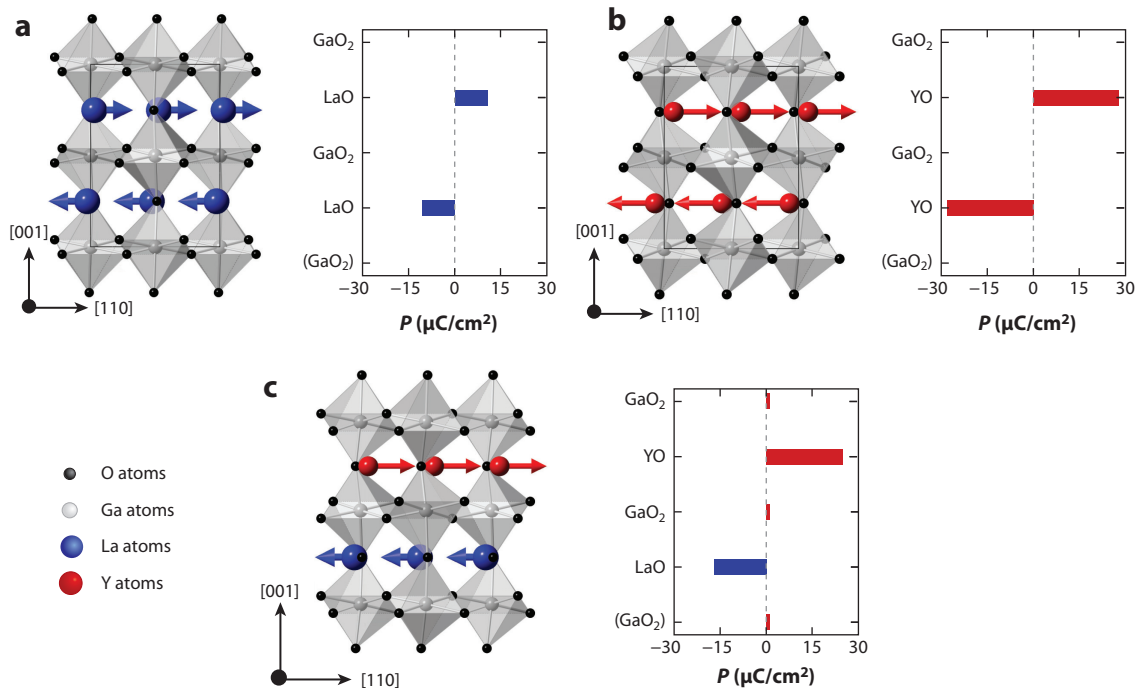


**Figure 4**

Layer-resolved polarization from first-principles calculations for (a)  $\text{LaGaO}_3$  in the  $Pnma$  space group, (b)  $\text{YGaO}_3$  in the  $Pnma$  space group, and (c)  $A$ -site cation-ordered  $\text{LaYGa}_2\text{O}_6$  double perovskite in the polar  $Pmc2_1$  space group. Figure adapted with permission from Reference 15; copyright 2012 Elsevier.

The crystal chemical origin of hybrid improper ferroelectricity in Dion–Jacobson phases is slightly different from that of  $A$ -site ordered double perovskites and Ruddlesden–Popper phases (74). In these materials, octahedral rotations and tilts also play a key role in establishing the polar ground state, which features dipoles in both the  $A$ –O and  $B$ –O layers. However, these dipoles are all aligned in the same direction, so the macroscopic polarization does not arise from a noncancellation of layer polarizations. The magnitude of the induced layer polarizations is correlated with the magnitude of the rotation distortions, which increase as the underbonding at the  $A$ -site in the high-symmetry  $P4/mmm$  parent structure increases. In contrast, the  $A'$  cation (usually an alkali cation) appears to contribute very little to the total macroscopic polarization.

### 3. SYNTHETIC ROUTES TO TRILINEARLY COUPLED POLAR AND FERROELECTRIC MATERIALS

#### 3.1. Cation-Ordered Perovskite Oxides

As noted above, although the octahedral rotations commonly associated with trilinearly coupled ferroelectricity are prevalent in  $ABO_3$  perovskite oxides, the 3D connectivity of the  $BO_6$  units in the perovskite structure prevents octahedral rotations alone from causing a macroscopic electrical polarization (16). However, if octahedral rotations are combined with cation order, ferroelectric behavior can be induced into the perovskite framework. For example, if the  $a^-a^+c^+$  tilting distortion observed in a large number of perovskite oxides is combined with layered  $A$ -cation order, as shown in **Figure 4**, macroscopic electrical polarizations can result.

Unfortunately the preparation of cation-ordered perovskite oxides is challenging. This is principally because at the high synthesis temperatures required for the preparation of most complex metal oxides, cation-disordered phases are strongly entropically preferred. However, cation-ordered phases can be favored thermodynamically if the cations being ordered have large differences in charge and/or size (82, 83). In the specific case of trilinearly coupled ferroelectric perovskites, the requirement for a layered ordering of the *A*-cations adds an additional difficulty, as layered ordering patterns tend to be disfavored compared with a 3D rock-salt ordering.

Knapp & Woodward (84) observed that it is possible to stabilize layered *A*-cation order if it is accompanied by *B*-site rock-salt order in an  $AA'BB'O_6$  double-double perovskite structure, so long as one of the *B*-cations is a  $d^0$  transition metal cation subject to a strong SOJT distortion as shown in **Figure 5**. However, of the growing number of suitably cation-ordered phases reported,

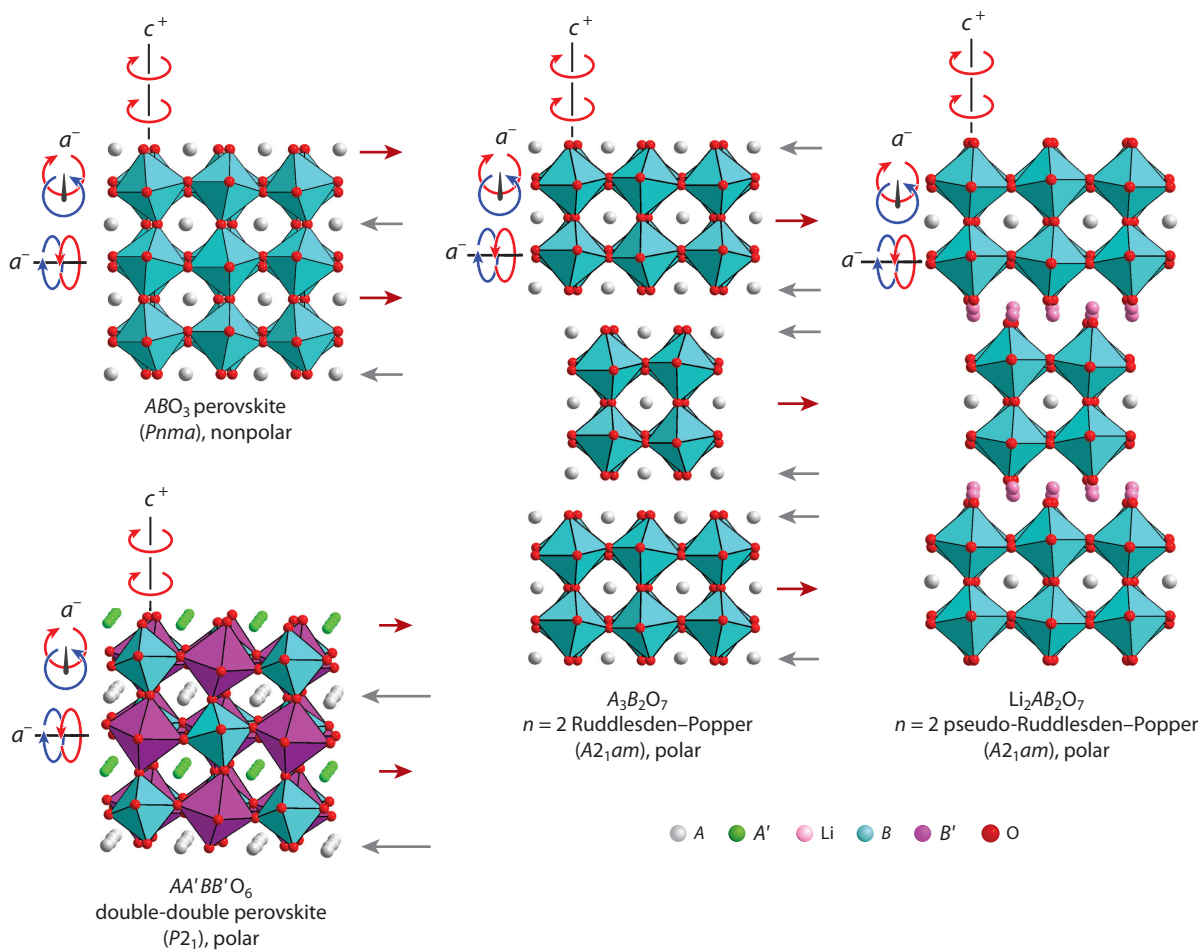


**Figure 5**

$AA'BB'O_6$  double-double perovskites can adopt  $P2_1$  symmetry polar structures, in contrast to nonpolar  $ABO_3$  phases. However, by breaking the 3D connectivity of the perovskite lattice, the *A*-cation displacements in  $n = 2$  Ruddlesden-Popper and pseudo-Ruddlesden-Popper phases no longer fully cancel, allowing a macroscopic polarization in the absence of cation order. Straight red and gray arrows indicate the *A*-cation displacements. Curved arrows indicate the sense of the octahedral rotations.

the majority adopt an  $a^-a^-c^0$  (space group  $P2_1/m$ ) tilting scheme rather than the desired  $a^-a^-c^+$  (space group  $P2_1$ ) arrangement (85, 86). The sparsity of  $P2_1$  symmetry phases can be attributed to the limited number of  $A$ - and  $B$ -cation quartets that have a suitable size and charge difference between  $A$  and  $A'$  and  $B$  and  $B'$  to stabilize cation order while simultaneously having a suitable difference in the average size of the  $A/A'$  and  $B/B'$  cations to stabilize an  $a^-a^-c^+$  tilting distortion and have one of the  $B$ -site cations be a  $d^0$  ion with a strong SOJT distortion.

There are compositions that do satisfy this lengthy list of strict criteria, which are observed to crystallize with polar  $P2_1$  symmetry. The most widely studied are phases of composition  $\text{NaLnMnWO}_6$  ( $Ln = \text{La, Nd, Tb}$ ) (45–47), which are predicted computationally to exhibit large ferroelectric polarizations (11). However, detailed physical measurements provide no indication of ferroelectric behavior, and other physical signatures of a noncentrosymmetric structure [piezoelectricity, second harmonic generation (SHG)] are weak, suggesting that any polarization present in the materials is small (48). By utilizing high-pressure, high-temperature synthesis,  $P2_1$  symmetry  $\text{NaYMnWO}_6$  can be stabilized, and while low-temperature polarization–electric field loops show no indication of ferroelectric behavior, dielectric and pyroelectric measurements are consistent with a change in a nonswitchable polarization at the magnetic ordering temperature of the phase ( $T_N = 8 \text{ K}$ ) (87).

The related  $\text{NaLnFeWO}_6$  ( $Ln = \text{La, Nd, Pr, Sm}$ ) iron compounds are also observed to adopt cation-ordered,  $a^-a^-c^+$  distorted polar structures, with the  $P2_1$  symmetry of the La and Nd phases confirmed by an unambiguous SHG signal (49, 50). However, as with the manganese phases, dielectric and polarization measurements show no indication of ferroelectric behavior in any of the four iron compounds.

By utilizing high-pressure, high-temperature synthesis conditions, it is possible to extend the stability range of the  $\text{NaLnMWO}_6$  double-double perovskite structure to include  $M = \text{Co}$  and  $\text{Ni}$ . Crystallographic analysis and SHG data reveal that  $\text{NaLnCoWO}_6$  phases with  $Ln = \text{Sm–Er, Y, and Yb}$  adopt polar  $P2_1$  structures (51, 52). To date the only phase that has been physically characterized in detail is  $\text{NaHoCoWO}_6$ , which, like  $\text{NaYMnWO}_6$ , shows no indication of ferroelectric behavior but does exhibit a change in a nonswitchable polarization at its magnetic ordering temperature ( $T_N = 8 \text{ K}$ ) (87). High-pressure synthesis also allows the preparation of  $\text{NaLnNiWO}_6$  phases with almost all the rare earth cations (53, 54). Phases containing large rare earths ( $Ln = \text{La–Tb}$ ) are polar (space group  $P2_1$ ) but nonswitchable with no observable dielectric anomaly at their magnetic ordering temperatures (54).  $\text{NaLnNiWO}_6$  phases with small rare earths ( $Ln = \text{Y, Dy, Ho, Yb}$ ) are also polar and pyroelectric at room temperature. However, on cooling below their magnetic ordering temperatures, there is a large change in the polarization, which is switchable in an applied electric field and exhibits magnetoelectric coupling (53).

The scope within which to expand the chemical range of polar  $AA'BB'O_6$  double-double perovskite oxides appears limited. The need to retain a significant charge difference (at least two units) between the  $A$  and  $A'$  cations, while retaining a small average  $A$ -cation size (to retain a small tolerance factor), restricts the  $A$ -cation choice to  $\text{Na–Ln}$  combinations, with small  $Ln^{3+}$  cations being preferred. Similarly, the choice of  $B$ -cations is also restricted by a requirement for a large  $B–B'$  charge difference while maintaining a large average  $B$ -cation size (again to retain a small tolerance factor). As a result even subtle changes, such as replacing  $W$  with  $Mo$  or using  $M^{III}$ ,  $M^V$   $B$ -site combinations in compounds such as  $\text{NaLaM}^{III}M^V\text{O}_6$  ( $M^{III} = \text{In, Mn, Fe}$ ;  $M^V = \text{Nb, Ta}$ ), destabilize either the cation order or the long-range  $a^-a^-c^+$  tilting distortion, leading to nonpolar materials (88–91).

The construction of artificial superlattices consisting of alternating layers of  $ABO_3$  and  $A'BO_3$  perovskite phases offers a way to sidestep the problems associated with stabilizing layer-ordered  $AA'B_2O_6$  double perovskite phases. By using epitaxy to sequentially deposit layers of  $ABO_3$  and

$A'BO_3$  perovskites, it is possible, in principle, to construct kinetically stable heterostructures that have the correct  $A$ -site cation order and octahedral rotations to exhibit hybrid improper ferroelectric behavior (92–94).

In practice, the mobility of species during the deposition process leads to some mixing of the  $A$  and  $A'$  cations, preventing the formation of heterostructures with sharp interfaces. However, Alaria et al. (95) have demonstrated that if an alternating sequence of five-layer blocks of  $\text{LaFeO}_3$  and  $\text{YFeO}_3$  is deposited onto a  $\text{DyScO}_3$  substrate, the resulting superlattice exhibits an approximately sinusoidal variation in La/Y occupancy with a 10-layer repeat length parallel to the deposition direction. This modulation in the La/Y occupancy is sufficient, when combined with octahedral tilting, to induce a polar distortion to the superlattice, as observed by SHG and piezoelectric measurements.

### 3.2. $n = 2$ Ruddlesden–Popper Oxides

The difficulties associated with stabilizing cation-ordered frameworks can be avoided by changing from the 3D perovskite structure to one of the layered perovskite variants that has an even number of perovskite sheets in its repeat unit. By breaking the 3D connectivity of the framework in this way, the  $BO_6$  octahedra are no longer forced to rotate in a fully reciprocal manner, and as a result the local polarizations due to  $A$ -cation displacements are no longer forced to fully cancel, allowing macroscopic polarizations in the absence of cation order, as shown in **Figure 5**.

By following this rationale, a number of  $A_3B_2O_7$ ,  $n = 2$  Ruddlesden–Popper oxides have been shown to exhibit switchable ferroelectric behavior driven by a trilinear coupling mechanism. The first experimental observation of hybrid improper ferroelectric behavior was achieved by measurements performed on single crystal samples of  $(\text{Ca}, \text{Sr})_3\text{Ti}_2\text{O}_7$ , which confirmed prior computational predictions (12, 59). This was followed by reports of ferroelectric behavior for  $(\text{Ca}, \text{Sr})_3\text{Sn}_2\text{O}_7$  (61),  $\text{Sr}_3\text{Zr}_2\text{O}_7$  (60), and  $\text{Ca}_3\text{Mn}_2\text{O}_7$  (58). All four compounds adopt  $a^-a^-c^+/a^-a^-c^+$  distorted,  $n = 2$  Ruddlesden–Popper structures described in space group  $A2_1am$  with the polar structures arising from a trilinear coupling of  $X_3^-$  ( $a^-a^-c^+/a^-a^-c^0$ ) and  $X_2^+$  ( $a^0a^0c^+/a^0a^0c^+$ ) tilting modes with the  $\Gamma_5^-$  polar mode, as predicted computationally (12).

In contrast to the well-established hybrid improper ferroelectric behavior of the four phases described above, there is some disagreement over the origin of the polar crystal structures of a series of  $\text{Li}_2\text{AB}_2\text{O}_7$  ( $A = \text{Sr}, \text{Ca}; B = \text{Nb}, \text{Ta}$ ) pseudo-Ruddlesden–Popper phases in which the  $\text{Li}^+$  cations reside in tetrahedral coordination sites rather than the nine-coordinate sites that are occupied in conventional Ruddlesden–Popper frameworks (**Figure 5**). Uppuluri et al. (62) reported that at room temperature  $\text{Li}_2\text{SrNb}_2\text{O}_7$  adopts a polar structure described in space group  $A2_1am$  with an  $a^-a^-c^+/a^-a^-c^+$  octahedral tilting pattern consistent with trilinear coupling, which on cooling below 90 K changes to an  $a^-a^-c^+/a^-a^-c^+$  antiferroelectric phase with  $Pnma$  symmetry. In contrast Nagai et al. (96, 97) reported that  $\text{Li}_2\text{SrNb}_2\text{O}_7$  adopts a nonpolar phase at room temperature, described in space group  $Amam$  with an  $a^-a^-c^0/a^-a^-c^0$  tilting pattern, which on cooling changes to a polar phase described in space group  $P2_1cn$  in which the polar structure is attributed to a proper ferroelectric mechanism involving Nb off-centering.  $\text{Li}_2\text{CaTi}_2\text{O}_7$  is reported to adopt a polar  $P2_1cn$  symmetry structure at room temperature (98). These conflicting reports highlight the challenge of unambiguously determining the subtle structural distortions that are responsible for ferroelectric behavior (trilinearly coupled or otherwise) and suggest that hybrid improper ferroelectricity and proper ferroelectricity involving SOJT  $d^0$  cations could be in competition in these materials. This competition between proper ferroelectricity and a trilinear coupling stabilization mechanism of polar structures can also be seen in a pair of  $A_2\text{La}(\text{TaTi})\text{O}_7$  ( $A = \text{Li}, \text{Na}$ ) phases (65). The pseudo-Ruddlesden–Popper phase  $\text{Li}_2\text{La}(\text{TaTi})\text{O}_7$

adopts an  $a^-a^-c^+/a^-a^-c^+$  distorted structure (space group  $A2_1am$ ) consistent with trilinear coupling. However, replacing the  $\text{Li}^+$  cations with larger  $\text{Na}^+$  cations yields a conventional Ruddlesden–Popper phase  $\text{Na}_2\text{La}(\text{TaTi})\text{O}_7$  with an  $a^-a^-c^-/a^-a^-c^-$  distortion (space group  $Pna2_1$ ) consistent with a polar structure stabilized by zone-center displacements of SOJT cations. Thus by controlling the size of the  $A'$ -cation in these  $A'_2AB_2\text{O}_7$  phases, the tilting pattern of the  $AB_2\text{O}_7$  perovskite double layers can be tuned to favor either a trilinear-coupling-stabilized polar structure or a polar structure stabilized simply by displacements of SOJT cations.

The list of reported hybrid improper ferroelectric  $n = 2$  Ruddlesden–Popper oxides is currently limited to the handful of compounds described above. At first sight the lifting of the cation-order requirement that applies to  $AB\text{O}_3$  perovskite phases suggests that there should be a large number of trilinearly coupled ferroelectric phases with  $n = 2$  Ruddlesden–Popper structures that can be prepared, further suggesting that there are many yet to be discovered. However, a more detailed analysis reveals that this is unlikely to be the case because in order to induce one of the four tilting schemes that lead to a trilinearly coupled polar structure, a very small structural tolerance factor,  $t$ , is required. We can crudely quantify this requirement by making use of the observation by Yoshida et al. (61) that the Curie temperature,  $T_c$ , of  $n = 2$  Ruddlesden–Popper hybrid improper ferroelectrics is proportional to  $t$  if, rather unusually, the tolerance factor is calculated using six-coordinate radii for both the  $A$ - and  $B$ -cations. Working backward from this observation reveals that for  $T_c > 0$  K,  $t < 0.88$  and for  $T_c > 300$  K,  $t < 0.87$ . Applying this to  $\text{Sr}_3B^{\text{IV}}_2\text{O}_7$  compositions reveals a minimum  $B^{\text{IV}}$  radius of 0.66 Å for  $T_c > 0$  K or 0.68 Å for  $T_c > 300$  K. Comparing these limits with tabulated ionic radii reveals that only five cations are sufficiently large:  $\text{Zr}^{4+}$  and  $\text{Sn}^{4+}$ , two known hybrid improper ferroelectrics;  $\text{Hf}^{4+}$ , which is computationally predicted to be a hybrid improper ferroelectric in  $\text{Sr}_3\text{Hf}_2\text{O}_7$  (99, 100); and  $\text{Nb}^{4+}$  and  $\text{Ta}^{4+}$ , which are not typically stable in extended oxides. Changing to  $\text{Ca}_3B^{\text{IV}}_2\text{O}_7$  or  $\text{Ln}_2\text{CaB}^{\text{III}}_2\text{O}_7$  compositions broadens the range of  $B$ -cations that can be included. However, the compositional range of polar  $n = 2$  Ruddlesden–Popper oxides is also restricted by the observation that  $A_3B_2\text{O}_7$  compositions are always in competition with a mixture of  $AB\text{O}_3$  and  $A_2BO_4$  phases, with this latter combination typically favored when  $t$  is small.

The general instability of  $n = 2$  Ruddlesden–Popper oxides with small tolerance factors is clearly evident in a study by Pitcher et al. (64) in which a series of  $\text{Ln}_2\text{A}^{\text{II}}\text{Fe}_2\text{O}_7$  phases was prepared so the structural evolution of the  $n = 2$  Ruddlesden–Popper framework could be tracked with declining tolerance factor. The study showed that  $\text{La}_2\text{SrFe}_2\text{O}_7$  adopts an undistorted aristotype  $n = 2$  Ruddlesden–Popper structure. Replacing  $\text{La}^{3+}$  with the smaller  $\text{Tb}^{3+}$  induces an  $a^-b^0c^0/b^0a^-c^0$  tilting distortion. However the synthesis of  $\text{Tb}_2\text{CaFe}_2\text{O}_7$ , which had been predicted computationally to adopt a polar  $a^-a^-c^+/a^-a^-c^+$  distorted structure, was not possible due to its separation into an  $n = 1$  Ruddlesden–Popper phase and a perovskite phase. In order to prepare a compound with the desired  $a^-a^-c^+/a^-a^-c^+$  distorted structure,  $(\text{Ca}_{0.6}\text{Sr}_{0.4})_{1.15}\text{Tb}_{1.85}\text{Fe}_2\text{O}_7$ , the most distorted all-iron phase that could be prepared, was mixed with  $\text{Ca}_3\text{Ti}_2\text{O}_7$  to both reduce the tolerance factor of the resulting material and stabilize the highly distorted structural framework. It was observed that around 15 mol%  $\text{Ca}_3\text{Ti}_2\text{O}_7$  was required to stabilize a polar distortion, and the resulting material showed a magnetoelectric coupling between the ordered magnetic moment of the phase and its electrical polarization.

### 3.3. $n = 2$ Dion–Jacobson Oxides

The  $A'AB_2\text{O}_7$   $n = 2$  Dion–Jacobson structure consists of  $AB_2\text{O}_7$  perovskite double layers, which are stacked in a primitive manner separated by large eight-coordinate  $A'$ -cations, typically  $\text{Cs}^+$  or  $\text{Rb}^+$  (101, 102). Theory and computational analysis have shown that the  $n = 2$  Dion–Jacobson

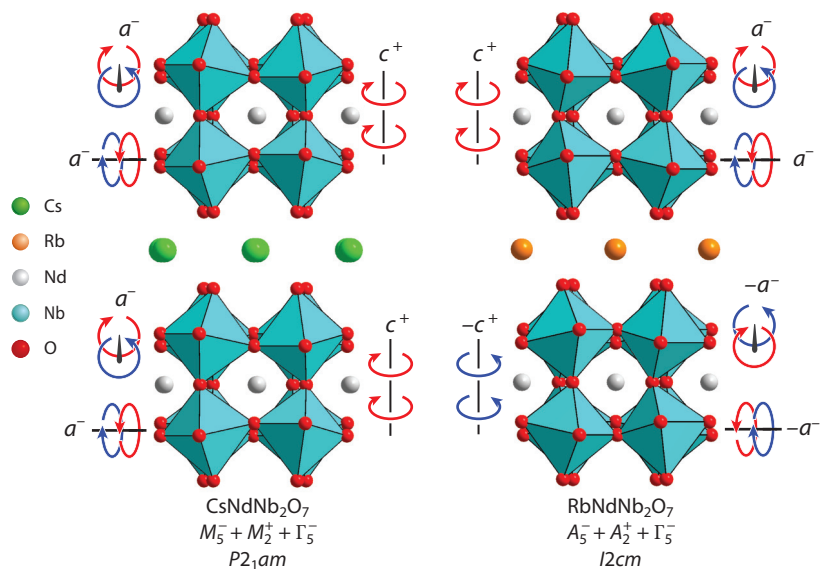


**Figure 6**

The polar structures of the Dion–Jacobson phases  $\text{CsNdNb}_2\text{O}_7$  and  $\text{RbNdNb}_2\text{O}_7$ , which adopt subtly different tilting distortions driven by a balance between satisfying the  $A'$ -cation coordination requirements and minimizing anion–anion repulsion.

structure can adopt trilinearly coupled polar configurations with the correct combination of  $A'$ -,  $A$ -, and  $B$ -cations (74). Indeed, first-principles calculations indicate that for a number of Dion–Jacobson phases, including  $\text{CsBiNb}_2\text{O}_7$ ,  $\text{CsLaNb}_2\text{O}_7$ , and  $\text{CsNdNb}_2\text{O}_7$ , the ground-state, lowest-energy structures should involve a trilinear coupling of  $M_5^-$  ( $a^-a^-c^0$ ) and  $M_2^+$  ( $a^0a^0c^+$ ) tilting distortions with a  $\Gamma_5^-$  polar mode to yield a polar structure described in space group  $P2_1am$  (74).

A combination of crystallography and polarization measurements has shown that both  $\text{CsBiNb}_2\text{O}_7$  and  $\text{RbBiNb}_2\text{O}_7$  adopt the predicted  $P2_1am$  symmetry structure and exhibit a switchable, spontaneous electrical polarization, characteristic of ferroelectric behavior, below Curie temperatures of  $T_c = 1,306$  K and 1,371 K for  $\text{CsBiNb}_2\text{O}_7$  and  $\text{RbBiNb}_2\text{O}_7$ , respectively (66, 67, 69).

Crystallographic measurements indicate that  $\text{CsNdNb}_2\text{O}_7$  and  $\text{CsNdTa}_2\text{O}_7$  also adopt polar  $P2_1am$  symmetry structures below  $T_c = 330$  K and 625 K, respectively, although ferroelectric behavior has been demonstrated only for  $\text{CsNdNb}_2\text{O}_7$  (66, 68, 103). The analogous Rb compounds,  $\text{RbNdNb}_2\text{O}_7$  and  $\text{RbNdTa}_2\text{O}_7$ , also adopt hybrid improper polar structures below  $T_c = 790$  K and 550 K, respectively (68, 103). However, the polarity of the Rb phases arises from a trilinear coupling of more complex  $A_5^-$ ,  $a^-a^-c^0 / -(a^-a^-c^0)$  and  $A_2^+$ ,  $a^0a^0c^+ / a^0a^0c^+$  tilting modes with the  $\Gamma_5^-$  polar mode, resulting in an  $a^-a^-c^+ / -(a^-a^-c^+)$  distorted structure described in space group  $I2cm$ , in which the direction of the  $a^-a^-c^+$  tilting distortion inverts between neighboring layers as shown in **Figure 6**. The differing structures of  $\text{CsNdM}_2\text{O}_7$  and  $\text{RbNdM}_2\text{O}_7$  are attributed to the compromise between optimizing the bonding of the  $A'$ -cation and minimizing oxide–oxide repulsion having different optimal solutions for the different  $A'$ -cations (68).

The behavior of the Dion–Jacobson phases  $\text{CsLaM}_2\text{O}_7$  and  $\text{RbLaM}_2\text{O}_7$  ( $M = \text{Nb}, \text{Ta}$ ) is less clear. Room-temperature measurements reveal that all four compounds are SHG active and piezoelectric (70). However, synchrotron X-ray diffraction data collected from  $\text{CsLaNb}_2\text{O}_7$  are incompatible with the  $P2_1am$  symmetry structure, which is calculated to be of the lowest energy. On the balance of evidence,  $\text{CsLaNb}_2\text{O}_7$  is actually thought to adopt a polar  $Amm2$  symmetry structure

that arises from a coupling of  $M_5^-, a^-b^0c^0$  and  $M_2^+, a^0a^0c^+$  tilting modes with an as yet undetermined  $\Gamma$ -point polar mode.

The  $A'AB_2O_7$  formulation of the  $n = 2$  Dion–Jacobson structure, combined with the requirement that the  $A'$ -cation be a large monovalent cation, limits the chemical diversity of compounds that adopt this structure type. Size and charge balancing requirements practically limit thermodynamically stable Dion–Jacobson oxide phases to compositions where  $A' = \text{Rb}^+$  or  $\text{Cs}^+$ ;  $A = \text{Bi}^{3+}$ ,  $\text{La}^{3+}$ ,  $\text{Ce}^{3+}$ ,  $\text{Pr}^{3+}$ , or  $\text{Nd}^{3+}$ ; and  $B = \text{Nb}^{5+}$  or  $\text{Ta}^{5+}$ , although it should be noted that  $A'\text{Bi}_2\text{Ta}_5\text{O}_{15}$  phases cannot be prepared due to the stability of the competing defect pyrochlore  $A'\text{Bi}_2\text{Ta}_5\text{O}_{15}$  phases (104). In principle  $A = \text{Sr}^{2+}$ ,  $B = \text{Nb}^{5+}/\text{W}^{6+}$  or  $\text{Ta}^{5+}/\text{W}^{6+}$  combinations can also form Dion–Jacobson structures, but even with the addition of these compositions, the number of complex oxides that can be made directly and adopt  $n = 2$  Dion–Jacobson structures is small.

The compositions of Dion–Jacobson phases can readily be modified via the extensive cation-exchange chemistry these compounds exhibit (105–107). For example the  $A'$ -cations in Dion–Jacobson phases can readily be exchanged for other monovalent cations (108–110), metal halides and sulphides (111–113), and a range of molecular species (114–116). Utilizing this approach, researchers have converted  $\text{RbNd}M_2\text{O}_7$  ( $M = \text{Nb}, \text{Ta}$ ) to the corresponding  $\text{LiNd}M_2\text{O}_7$  compounds via Li-for-Rb cation exchange (63, 108, 110). Crystallographic analysis reveals that  $\text{LiNdNb}M_2\text{O}_7$  and  $\text{LiNdTa}M_2\text{O}_7$  adopt polar pseudo-Ruddlesden–Popper type structures in which the lithium cations adopt an ordered arrangement within tetrahedral sites located between the  $\text{Nd}M_2\text{O}_7$  perovskite double sheets. The polarity of the  $\text{LiNd}M_2\text{O}_7$  phases arises from a coupling of  $X_4^-, a^-a^-c^0 / -(a^-a^-)c^0$  and  $X_2^+, a^0a^0c^+ / a^0a^0 - c^+$  tilting distortions with a  $\Gamma_4^-$  polar mode to yield an  $a^-a^-c^+ / -(a^-a^-c^+)$  distorted structure described in space group  $B2cm$  (63).

### 3.4. $n = 2$ Aurivillius Phase Oxides

Aurivillius phases have structures in which perovskite blocks are separated by  $(\text{Bi}_2\text{O}_2)^{2+}$  slabs in a repeating stacking sequence. Thus, an  $n = 2$  Aurivillius phase has a general formula of  $(\text{Bi}_2\text{O}_2)AB_2\text{O}_7$  and, like the related Ruddlesden–Popper and Dion–Jacobson phases, contains perovskite double sheets, which can undergo analogous tilting distortions that can break inversion symmetry to yield polar structures stabilized by a trilinear coupling mechanism. The two most studied  $n = 2$  Aurivillius phases are  $(\text{Bi}_2\text{O}_2)\text{SrTa}_2\text{O}_7$  and  $(\text{Bi}_2\text{O}_2)\text{SrNb}_2\text{O}_7$  (55–57). Both of these materials are observed to adopt undistorted structures at high temperature (space group  $I4/mmm$ ) and polar structures at room temperature (space group  $A2_1am$ ). The polar ground states of the two  $(\text{Bi}_2\text{O}_2)\text{Sr}M_2\text{O}_7$  phases adopt  $a^-a^-c^+ / a^-a^-c^+$  tilting distortions, which arise from a combination of  $X_3^-, a^-a^-c^0 / a^-a^-c^0$  and  $X_2^+, a^0a^0c^+ / a^0a^0c^+$  distortion modes that then couple to a  $\Gamma_5^-$  polar mode (9, 117) in a manner directly analogous to that observed for  $n = 2$  Ruddlesden–Popper phases (12). An interesting difference between  $(\text{Bi}_2\text{O}_2)\text{SrTa}_2\text{O}_7$  and  $(\text{Bi}_2\text{O}_2)\text{SrNb}_2\text{O}_7$  is that the former material undergoes two phase transitions on cooling, first from the  $I4/mmm$  aristotype phase to an  $Amam$  symmetry phase (consistent with the freezing of the  $X_3^-$  mode) (56) and then to the polar  $A2_1am$  ground state. In contrast,  $(\text{Bi}_2\text{O}_2)\text{SrNb}_2\text{O}_7$  appears to undergo only a single phase transition directly from the  $I4/mmm$  aristotype to the  $A2_1am$  polar ground state. This difference is attributed to a much stronger trilinear coupling among the  $X_3^-, X_2^+$ , and  $\Gamma_5^-$  modes in the Nb phase, which suppresses the appearance of the  $Amam$  intermediate (117).

In common with the Ruddlesden–Popper and Dion–Jacobson phases, the required charge balance for  $(\text{Bi}_2\text{O}_2)A^{n+}B_2^{m+}\text{O}_7$ ,  $n = 2$  Aurivillius phases ( $n + 2m = 12$ ) restricts the chemical diversity of compositions that can adopt this structure before even considering the relative sizes of the  $A$ - and  $B$ -cations required to stabilize the required tilting distortions. Thus it is no real surprise that there are few known compositions that adopt  $n = 2$  Aurivillius structures and little scope for preparing more.

### 3.5. Future Directions

The examples detailed above show that it is possible for complex oxides to exhibit robust hybrid improper ferroelectric behavior. However, in studying these materials it has become clear that the large magnitudes of the nonpolar tilting distortions associated with this behavior in layered perovskites limit the chemical diversity of phases that can exhibit polar distortions stabilized by trilinear coupling. Indeed, the rudimentary analysis described above suggests that the majority of thermodynamically stable hybrid improper ferroelectric oxides have already been discovered.

One promising option to expand the range of hybrid improper ferroelectric materials is to move beyond thermodynamically stable phases and investigate metastable materials. *Chimie douce*, or soft chemical, synthesis approaches offer routes for the preparation of novel materials where the products are selected under kinetic control rather than on the basis of thermodynamic stability (105–107). Many layered oxides, such as Dion–Jacobson or Ruddlesden–Popper phases, exhibit facile, topochemical cation exchange reactions, which yield metastable phases that cannot be prepared by conventional high-temperature synthetic methods. Such cation exchange reactions can be used to modify the structural tolerance factors of materials to tune them to values that induce hybrid improper ferroelectric behavior. For example, as noted above,  $\text{RbNdM}_2\text{O}_7$  ( $M = \text{Nb}, \text{Ta}$ ) Dion–Jacobson phases exhibit facile Li-for-Rb cation exchange reactions to yield the corresponding metastable, polar,  $\text{LiNdM}_2\text{O}_7$  pseudo-Ruddlesden–Popper phases (63). Analogous cation exchange reactions could be used to expand the range of hybrid improper ferroelectric materials significantly. Furthermore, such reactions can in principle allow aliovalent cation exchanges in which two monovalent cations are replaced by a divalent cation (119–121), allowing paramagnetic transition metal cations to be incorporated in these frameworks (122, 123) and offering a potential route to magnetoelectric materials.

Soft chemical routes can also be used to introduce additional anions into layered oxides to modify the tilting distortions of the host framework. For example,  $\text{La}_3\text{Ni}_2\text{O}_7$  adopts an  $n = 2$  Ruddlesden–Popper structure with a nonpolar  $a^-a^-c^0/a^-a^-c^0$  tilting distortion (124). Low-temperature oxidation with fluorine yields  $\text{La}_3\text{Ni}_2\text{O}_{5.5}\text{F}_{3.5}$ , which exhibits an  $a^-a^-c^+/a^-a^- - c^+$  antipolar tilting distortion (125), demonstrating that such topochemical oxidation reactions can be utilized to enhance the tilting distortions of layered complex oxides and in principle induce trilinearly coupled polar distortions.

A further option for expanding the family of hybrid improper ferroelectric oxide materials is to examine layered perovskite frameworks with  $n > 2$ . In general, the thermodynamic stability of layered perovskite variants declines as the thickness of the perovskite sheets increases, making the preparation of materials with  $n > 2$  challenging. However, these more complex layered materials can exhibit additional tilting distortion modes not possible in the analogous  $n = 2$  systems, so these systems can, in principle, exhibit a rich range of coupled distortions, with hybrid improper behavior reported for  $n = 3$  Aurivillius phases already (126).

In this review we have restricted ourselves to discussing all-oxide systems. However, the perovskite structure and its layered variants are adopted by a wide variety of chemical systems, including those with molecular components (127), such as the much-studied hybrid halide perovskites (128–130), and systems such as formates (131, 132), cyanides (133, 134), thiocyanates (135, 136), and azides (137, 138), where molecular units take the place of oxide anions. These molecular perovskites can undergo a range of tilting distortions, many of which have no analog in the all-oxide systems described here (139) and which can couple to and stabilize polar distortion modes (140). Thus, while we may conclude that most of the thermodynamically stable oxide hybrid improper ferroelectrics have probably already been discovered, the field is ripe for the discovery of a wider

range of new, more chemically diverse materials with polar structures stabilized by the trilinear coupling of polar and nonpolar distortion modes.

## DISCLOSURE STATEMENT

The authors are not aware of any affiliations, memberships, funding, or financial holdings that might be perceived as affecting the objectivity of this review.

## ACKNOWLEDGMENTS

N.A.B. was supported by National Science Foundation award DMR-1550347.

## LITERATURE CITED

1. Petzelt J, Dvořák V. 1971. Symmetry aspect of the phase transitions in boracites. *Czechoslov. J. Phys. B* 21:1141–52
2. Smollenskii GA, Siniĭ IG, Tagantsev AK, Prokhorova SD, Mikvabiya VD, Windsch W. 1985. Acoustic anomaly and nature of the phase transition in the uniaxial weakly polar ferroelectric TSSC. *Sov. Phys. JETP* 61:566–605
3. Tagantsev AK. 1987. Weakly polar ferroelectricity: dielectric properties and possible nature. *JETP Lett.* 45:447–50
4. Tagantsev AK. 1988. Weak ferroelectrics. *Ferroelectrics* 79:57–60
5. Levanyuk AP, Sannikov DG. 1974. Improper ferroelectrics. *Sov. Phys. Uspekhi* 17:199–214
6. Stokes HT, Hatch DM. 1991. Coupled order parameters in the Landau theory of phase transitions in solids. *Phase Transit.* 34:53–67
7. Aleksandrov KS. 1995. Structural phase transitions in layered perovskitelike crystals. *Crystallogr. Rep.* 40:251–72
8. Aleksandrov KS, Beznosikov VV. 1997. Hierarchies of perovskite-like crystals. *Phys. Solid State* 39:695–715
9. Etxebarria I, Perez-Mato JM, Boullay P. 2010. The role of trilinear couplings in the phase transitions of Aurivillius compounds. *Ferroelectrics* 401:17–23
10. Bousquet E, Dawber M, Stucki N, Lichtensteiger C, Hermet P, et al. 2008. Improper ferroelectricity in perovskite oxide artificial superlattices. *Nature* 452:732–36
11. Fukushima T, Stroppa A, Picozzi S, Perez-Mato JM. 2011. Large ferroelectric polarization in the new double perovskite NaLaMnWO<sub>6</sub> induced by non-polar instabilities. *Phys. Chem. Chem. Phys.* 13:12186–90
12. Benedek NA, Fennie CJ. 2011. Hybrid improper ferroelectricity: a mechanism for controllable polarization-magnetization coupling. *Phys. Rev. Lett.* 106:107204
13. Rabe KM, Dawber M, Lichtensteiger C, Ahn CH, Triscone JM. 2007. Modern physics of ferroelectrics: essential background. In *Physics of Ferroelectrics: A Modern Perspective*, ed. CH Ahn, pp. 1–30. Berlin: Springer-Verlag
14. Rabe KM, Ghosez P. 2007. First-principles studies of ferroelectric oxides. In *Physics of Ferroelectrics: A Modern Perspective*, ed. CH Ahn, pp. 117–74. Berlin: Springer-Verlag
15. Benedek NA, Mulder AT, Fennie CJ. 2012. Polar octahedral rotations: a path to new multifunctional materials. *J. Solid State Chem.* 195:11–20
16. Rondinelli JM, Fennie CJ. 2012. Octahedral rotation-induced ferroelectricity in cation ordered perovskites. *Adv. Mater.* 24:1961–68
17. Mulder AT, Benedek NA, Rondinelli JM, Fennie CJ. 2013. Turning ABO<sub>3</sub> antiferroelectrics into ferroelectrics: design rules for practical rotation-driven ferroelectricity in double perovskites and A<sub>3</sub>B<sub>2</sub>O<sub>7</sub> Ruddlesden-Popper compounds. *Adv. Funct. Mater.* 23:4810–20
18. Bellaiche L, Íñiguez J. 2013. Universal collaborative couplings between oxygen-octahedral rotations and antiferroelectric distortions in perovskites. *Phys. Rev. B* 88:014104

19. Zhao HJ, Íñiguez J, Ren W, Chen XM, Bellaiche L. 2014. Atomistic theory of hybrid improper ferroelectricity in perovskites. *Phys. Rev. B* 89:174101
20. Benedek NA, Rondinelli JM, Djani H, Ghosez P, Lightfoot P. 2015. Understanding ferroelectricity in layered perovskites: new ideas and insights from theory and experiments. *Dalton Trans.* 44:10543–58
21. Gu T, Scarbrough T, Yang Y, Íñiguez J, Bellaiche L, Xiang HJ. 2018. Cooperative couplings between octahedral rotations and ferroelectricity in perovskites and related materials. *Phys. Rev. Lett.* 120:197602
22. Salje EKH. 1992. Application of Landau theory for the analysis of phase transitions in minerals. *Phys. Rep.* 215:49–99
23. Chandra P, Littlewood PB. 2007. A Landau primer for ferroelectrics. In *Physics of Ferroelectrics: A Modern Perspective*, ed. CH Ahn, pp. 69–116. Berlin: Springer-Verlag
24. Cohen RE. 1992. Origin of ferroelectricity in perovskite oxides. *Nature* 358:136–38
25. Ghosez P, Cockayne E, Waghmare UV, Rabe KM. 1999. Lattice dynamics of BaTiO<sub>3</sub>, PbTiO<sub>3</sub> and PbZrO<sub>3</sub>: a comparative first-principles study. *Phys. Rev. B* 60:836–43
26. Cochran W. 1959. Crystal stability and the theory of ferroelectricity. *Phys. Rev. Lett.* 3:412–14
27. Cochran W. 1960. Crystal stability and the theory of ferroelectricity. *Adv. Phys.* 9:387–423
28. Van Aken BB, Palstra TTM, Filippetti A, Spaldin NA. 2004. The origin of ferroelectricity in magnetoelectric YMnO<sub>3</sub>. *Nat. Mater.* 3:164–70
29. Fennie CJ, Rabe KM. 2005. Ferroelectric phase transition in YMnO<sub>3</sub> from first principles. *Phys. Rev. B* 72:100103
30. Smolenskii GA, Bokov VA. 1964. Coexistence of magnetic and electric ordering in crystals. *J. Appl. Phys.* 35:915–18
31. Artyukhin S, Delaney KT, Spaldin NA, Mostovoy M. 2014. Landau theory of topological defects in multiferroic hexagonal manganites. *Nat. Mater.* 13:42–49
32. Choi T, Horibe Y, Yi HT, Choi YJ, Wu W, Cheong SW. 2010. Insulating interlocked ferroelectric and structural antiphase domain walls in multiferroic YMnO<sub>3</sub>. *Nat. Mater.* 9:253–58
33. Bersuker IB. 2001. Modern aspects of the Jahn–Teller effect theory and applications to molecular problems. *Chem. Rev.* 101:1067–114
34. Payne DJ, Egdell RG, Walsh A, Watson GW, Guo J, et al. 2006. Electronic origins of structural distortions in post-transition metal oxides: experimental and theoretical evidence for a revision of the lone pair model. *Phys. Rev. Lett.* 96:157403
35. Stoltzfus MW, Woodward PM, Seshadri R, Klepeis JH, Bursten B. 2007. Structure and bonding in SnWO<sub>4</sub>, PbWO<sub>4</sub>, and BiVO<sub>4</sub>: lone pairs versus inert pairs. *Inorg. Chem.* 46:3839–50
36. Walsh A, Payne DJ, Egdell RG, Watson GW. 2011. Stereochemistry of post-transition metal oxides: revision of the classical lone pair model. *Chem. Soc. Rev.* 40:4455–63
37. Seshadri R, Hill NA. 2001. Visualizing the role of Bi 6s “lone pairs” in the off-center distortion in ferromagnetic BiMnO<sub>3</sub>. *Chem. Mater.* 13:2892–99
38. Neaton JB, Ederer C, Waghmare UV, Spaldin NA, Rabe KM. 2005. First-principles study of spontaneous polarization in multiferroic BiFeO<sub>3</sub>. *Phys. Rev. B* 71:014113
39. Belik AA. 2012. Polar and nonpolar phases of BiMO<sub>3</sub>: a review. *J. Solid State Chem.* 195:32–40
40. Harrison WA. 1989. *Electronic Structure and the Properties of Solids: The Physics of the Chemical Bond*. New York: Dover
41. Ghosez P, Michenaud JP, Gonze X. 1998. Dynamical atomic charges: the case of ABO<sub>3</sub> compounds. *Phys. Rev. B* 58:6224–40
42. Spaldin NA. 2012. A beginner’s guide to the modern theory of polarization. *J. Solid State Chem.* 195:2–10
43. Ederer C, Spaldin NA. 2006. Origin of ferroelectricity in the multiferroic barium fluorides BaMF<sub>4</sub>: a first principles study. *Phys. Rev. B* 74:024102
44. Garcia-Castro AC, Spaldin NA, Romero AH, Bousquet E. 2014. Geometric ferroelectricity in fluoroperovskites. *Phys. Rev. B* 89:104107
45. King G, Wayman LM, Woodward PM. 2009. Magnetic and structural properties of NaLnMnWO<sub>6</sub> and NaLnMgWO<sub>6</sub> perovskites. *J. Solid State Chem.* 182:1319–25
46. King G, Wills AS, Woodward PM. 2009. Magnetic structures of NaLMnWO<sub>6</sub> perovskites (L=La, Nd, Tb). *Phys. Rev. B* 79:224428

47. King G, Thimmaiah S, Dwivedi A, Woodward PM. 2007. Synthesis and characterization of new  $AA'BWO_6$  perovskites exhibiting simultaneous ordering of  $A$ -site and  $B$ -site cations. *Chem. Mater.* 19:6451–58
48. De C, Kim TH, Kim KH, Sundaresan A. 2014. The absence of ferroelectric polarization in layered and rock-salt ordered  $NaLnMnWO_6$  ( $Ln = La, Nd, Tb$ ) perovskites. *Phys. Chem. Chem. Phys.* 16:5407–11
49. Blasco J, Rodriguez-Velamazán JA, Subías G, Garcia-Munoz JL, Stankiewicz J, Garcia J. 2019. Spin ordering and physical properties of  $NaPrFeWO_6$  and  $NaSmFeWO_6$  with polar double perovskite structure. *Acta Mater.* 176:53–62
50. Retuerto M, Li MR, Ignatov A, Croft M, Ramanujachary KV, et al. 2013. Polar and magnetic layered  $A$ -site and rock salt  $B$ -site-ordered  $NaLnFeWO_6$  ( $Ln = La, Nd$ ) perovskites. *Inorg. Chem.* 52:12482–91
51. Zuo P, Colin CV, Klein H, Bordet P, Suard E, et al. 2017. Structural study of a doubly ordered perovskite family  $NaLnCoWO_6$  ( $Ln = Y, La, Pr, Nd, Sm, Eu, Gd, Tb, Dy, Ho, Er, Yb$ ): hybrid improper ferroelectricity in nine new members. *Inorg. Chem.* 56:8478–89
52. Zuo P, Klein H, Darie C, Colin CV. 2018. Magnetic properties of the doubly ordered perovskite  $NaLnCoWO_6$  ( $Ln = Y, La, Pr, Nd, Sm, Eu, Gd, Tb, Dy, Ho, Er, Yb$ ) family. *J. Magn. Magn. Mater.* 458:48–51
53. Shankar PNR, Orlandi F, Manuel P, Zhang WG, Halasyamani PS, Sundaresan A. 2020.  $A$ -site and  $B$ -site cation ordering induces polar and multiferroic behavior in the perovskite  $NaLnNiWO_6$  ( $Ln = Y, Dy, Ho, and Yb$ ). *Chem. Mater.* 32:5641–49
54. Shankar PNR, Orlandi F, Manuel P, Zhang WG, Halasyamani PS, Sundaresan A. 2021. Structural, magnetic, and electrical properties of doubly ordered perovskites  $NaLnNiWO_6$  ( $Ln = La, Pr, Nd, Sm, Eu, Gd, and Tb$ ). *J. Phys. Chem. C* 125:6749–57
55. Snedden A, Hervoche CH, Lightfoot P. 2003. Ferroelectric phase transitions on  $SrBi_2Nb_2O_9$  and  $Bi_5Ti_3FeO_{15}$ : a powder neutron diffraction study. *Phys. Rev. B* 67:092102
56. Rae AD, Thompson JG, Withers RL. 1992. Structure refinement of commensurately modulated bismuth strontium tantalate,  $Bi_2SrTa_2O_9$ . *Acta Crystallogr.* B48:418–28
57. Boullay P, Tellier J, Mercurio D, Manier M, Zuniga FJ, Perez-Mato JM. 2012. Phase transition sequence in ferroelectric Aurivillius compounds investigated by single crystal X-ray diffraction. *Solid State Sci.* 14:1367–71
58. Liu MF, Zhang Y, Lin LF, Lin L, Yang SW, et al. 2018. Direct observation of ferroelectricity in  $Ca_3Mn_2O_7$  and its prominent light absorption. *Appl. Phys. Lett.* 113:022902
59. Oh YS, Luo X, Huang FT, Wang YZ, Cheong SW. 2015. Experimental demonstration of hybrid improper ferroelectricity and the presence of abundant charged walls in  $(Ca, Sr)_3Ti_2O_7$  crystals. *Nat. Mater.* 14:407–13
60. Yoshida S, Fujita K, Akamatsu H, Hernandez O, Sen Gupta A, et al. 2018. Ferroelectric  $Sr_3Zr_2O_7$ : competition between hybrid improper ferroelectric and antiferroelectric mechanisms. *Adv. Funct. Mater.* 28:1801856
61. Yoshida S, Akamatsu H, Tsuji R, Hernandez O, Padmanabhan H, et al. 2018. Hybrid improper ferroelectricity in  $(Sr,Ca)_3Sn_2O_7$  and beyond: universal relationship between ferroelectric transition temperature and tolerance factor in  $n = 2$  Ruddlesden-Popper phases. *J. Am. Chem. Soc.* 140:15690–700
62. Uppuluri R, Akamatsu H, Sen Gupta A, Wang HY, Brown CM, et al. 2019. Competing polar and antipolar structures in the Ruddlesden-Popper layered perovskite  $Li_2SrNb_2O_7$ . *Chem. Mater.* 31:4418–25
63. Zhu T, Khalsa G, Havas DM, Gibbs AS, Zhang W, et al. 2018. Cation exchange as a mechanism to engineer polarity in layered perovskites. *Chem. Mater.* 30:8915–24
64. Pitcher MJ, Mandal P, Dyer MS, Alaria J, Borisov P, et al. 2015. Tilt engineering of spontaneous polarization and magnetization above 300 K in a bulk layered perovskite. *Science* 347:420–24
65. Mallick S, Fortes AD, Zhang W, Halasyamani PS, Hayward MA. 2021. Switching between proper and hybrid-improper polar structures via cation substitution in  $A_2La(TaTi)O_7$  ( $A = Li, Na$ ). *Chem. Mater.* 33:2666–72
66. Snedden A, Knight KS, Lightfoot P. 2003. Structural distortions in the layered perovskites  $CsANb_2O_7$  ( $A = Nd, Bi$ ). *J. Solid State Chem.* 173:309–13
67. Li BW, Osada M, Ozawa TC, Sasaki T. 2012.  $RbBiNb_2O_7$ : a new lead-free high- $T_c$  ferroelectric. *Chem. Mater.* 24:3111–13

68. Zhu T, Cohen T, Gibbs AS, Zhang W, Halasyamani PS, et al. 2017. Theory and neutrons combine to reveal a family of layered perovskites without inversion symmetry. *Chem. Mater.* 29:9489–97
69. Chen C, Ning HP, Lepadatu S, Cain M, Yan HX, Reece MJ. 2015. Ferroelectricity in Dion–Jacobson  $ABiNb_2O_7$  ( $A = Rb, Cs$ ) compounds. *J. Mater. Chem. C* 3:19–22
70. Strayer ME, Sen Gupta A, Akamatsu H, Lei S, Benedek NA, et al. 2016. Emergent noncentrosymmetry and piezoelectricity driven by oxygen octahedral rotations in  $n = 2$  Dion–Jacobson phase layered perovskites. *Adv. Funct. Mater.* 26:1930–37
71. Nowadnick EA, Fennie CJ. 2016. Domains and ferroelectric switching pathways in  $Ca_3Ti_2O_7$  from first principles. *Phys. Rev. B* 94:104105
72. Stengel M, Fennie CJ, Ghosez P. 2012. Electrical properties of improper ferroelectrics from first principles. *Phys. Rev. B* 86:094112
73. Burdett JK. 1981. Use of the Jahn–Teller theorem in inorganic chemistry. *Inorg. Chem.* 20:1959–62
74. Benedek NA. 2015. Origin of ferroelectricity in a family of polar oxides: the Dion–Jacobson phases. *Inorg. Chem.* 53:3769–77
75. Glazer AM. 1972. The classification of tilted octahedra in perovskites. *Acta Crystallogr.* B28:3384–92
76. Megaw HD, Darlington CNW. 1975. Geometrical and structural relations in the rhombohedral perovskites. *Acta Crystallogr.* A31:161–73
77. Aleksandrov KS. 1976. Successive structural phase-transitions in perovskites. 1. Symmetry distorted phases. *Kristallografiya* 21:249–55
78. O’Keeffe M, Hyde BG. 1977. Some structures topologically related to cubic perovskite ( $E21$ ),  $ReO_3$  ( $D09$ ) and  $Cu_3Au$  ( $L12$ ). *Acta Crystallogr.* B33:3802–13
79. Woodward PM. 1997. Octahedral tilting in perovskites. I. Geometrical considerations. *Acta Crystallogr.* B53:32–43
80. Woodward PM. 1997. Octahedral tilting in perovskites. II. Structure stabilizing forces. *Acta Crystallogr.* B53:44–66
81. Howard CJ, Stokes HT. 1998. Group-theoretical analysis of octahedral tilting in perovskites. *Acta Crystallogr.* B54:782–89
82. Anderson MT, Greenwood KB, Taylor GA, Poeppelmeier KR. 1993. B-cation arrangements in double perovskites. *Prog. Solid State Chem.* 22:197–233
83. King G, Woodward PM. 2010. Cation ordering in perovskites. *J. Mater. Chem.* 20:5785–96
84. Knapp MC, Woodward PM. 2006. A-site cation ordering in  $AA'BB'O_6$  perovskites. *J. Solid State Chem.* 179:1076–85
85. Lopez ML, Veiga ML, Pico C. 1994. Cation ordering in distorted perovskites  $(MLa)(NgTe)O_6$ ,  $M = Na, K$ . *J. Mater. Chem.* 4:547–50
86. Arillo MA, Gomez J, Lopez ML, Pico C, Veiga ML. 1997. Structural characterization and properties of the perovskite  $(NaLa)(MW)O_6$  ( $M = Co, Ni$ ): two new members in the group–subgroup relations for the perovskite-type structures. *J. Mater. Chem* 7:801–6
87. De C, Sundaresan A. 2018. Nonswitchable polarization and magnetoelectric coupling in the high-pressure synthesized doubly ordered perovskites  $NaYMnWO_6$  and  $NaHoCoWO_6$ . *Phys. Rev. B* 97:214418
88. Dachraoui W, Yang T, Liu C, King G, Hadermann J, et al. 2011. Short-range layered  $A$ -site ordering in double perovskites  $NaLaBB'O_6$  ( $B = Mn, Fe$ ;  $B' = Nb, Ta$ ). *Chem. Mater.* 23:2398–406
89. King G, Garcia-Martin S. 2019. Expanding the doubly cation ordered  $AA'BB'O_6$  perovskite family: structural complexity in  $NaLaInNbO_6$  and  $NaLaInTaO_6$ . *Inorg. Chem.* 58:14058–67
90. Borchani SM, Koubaa WCR, Megdiche M. 2017. Structural, magnetic and electrical properties of a new double-perovskite  $LaNaMnMoO_6$  material. *R. Soc. Open Sci.* 4:10920
91. Borchani SM, Megdiche M. 2018. Electrical properties and conduction mechanism in the  $NaLaMnMoO_6$  double perovskite ceramic. *J. Phys. Chem. Solids* 114:121–28
92. Ghosh S, Fennie CJ. 2015. Linear magnetoelectricity at room temperature in perovskite superlattices by design. *Phys. Rev. B* 92:184112
93. Zhang YJ, Wang J, Sahoo MPK, Wang XY, Shimada T, Kitamura T. 2016. Hybrid improper ferroelectricity in  $SrZrO_3/BaZrO_3$  superlattice. *Phys. Chem. Chem. Phys.* 18:24024–32

94. Zhou PX, Lu SH, Li CF, Zhong CG, Zhao ZY, et al. 2019. Magnetism and hybrid improper ferroelectricity in  $\text{LaMO}_3/\text{YMO}_3$  superlattices. *Phys. Chem. Chem. Phys.* 21:20132–36
95. Alaria J, Borisov P, Dyer MS, Manning TD, Lepadatu S, et al. 2014. Engineered spatial inversion symmetry breaking in an oxide heterostructure built from isosymmetric room-temperature magnetically ordered components. *Chem. Sci.* 5:1599–610
96. Nagai T, Mochizuki Y, Shirakuni H, Nakano A, Oba F, et al. 2020. Phase transition from weak ferroelectricity to incipient ferroelectricity in  $\text{Li}_2\text{Sr}(\text{Nb}_{1-x}\text{Ta}_x)_2\text{O}_7$ . *Chem. Mater.* 32:744–50
97. Nagai T, Shirakuni H, Nakano A, Sawa H, Moriwake H, et al. 2019. Weak ferroelectricity in  $n = 2$  pseudo Ruddlesden–Popper-type niobate  $\text{Li}_2\text{SrNb}_2\text{O}_7$ . *Chem. Mater.* 31:6257–61
98. Zhang BH, Hu ZZ, Chen BH, Liu XQ, Chen XM. 2020. Room-temperature ferroelectricity in  $A$ -site ordered Ruddlesden–Popper  $\text{Li}_2\text{CaTa}_2\text{O}_7$  ceramics. *J. Mater. Chem.* 6:593–99
99. da Silva EL, Gerami AM, Lekshmi PN, Marcondes ML, Assali LVC, et al. 2021. Group theory analysis to study phase transitions of quasi-2D  $\text{Sr}_3\text{Hf}_2\text{O}_7$ . *Nanomaterials* 11:897
100. Liu XQ, Lu JJ, Chen BH, Zhang BH, Chen XM. 2019. Hybrid improper ferroelectricity and possible ferroelectric switching paths in  $\text{Sr}_3\text{Hf}_2\text{O}_7$ . *J. Appl. Phys.* 125:114105
101. Dion M, Ganne M, Tournoux M. 1981. The new phase families  $M^I M_2^{II} \text{Nb}_3\text{O}_{10}$  with perovskite sheets. *Mater. Res. Bull.* 16:1429–35
102. Jacobson AJ, Johnson JW, Lewandowski JT. 1985. Interlayer chemistry between thick transition-metal oxide layers: synthesis and intercalation reactions of  $\text{KCa}_2\text{Na}_{n-3}\text{Nb}_n \text{O}_{3n+1}$  ( $3 < n < 7$ ). *Inorg. Chem.* 24:3727–29
103. Zhu T, Gibbs AS, Benedek NA, Hayward MA. 2020. Complex structural phase transitions of the hybrid improper polar Dion–Jacobson oxides  $\text{RbNdM}_2\text{O}_7$  and  $\text{CsNdM}_2\text{O}_7$  ( $M = \text{Nb, Ta}$ ). *Chem. Mater.* 32:4340–46
104. Ehlert MK, Greedan JE, Subramanian MA. 1988. Novel defect pyrochlores  $\text{ABi}_2\text{B}_5\text{O}_{16}$  ( $A = \text{Cs, Rb}$ ;  $B = \text{Ta, Nb}$ ). *J. Solid State Chem.* 75:188–96
105. Schaak RE, Mallouk TE. 2002. Perovskites by design: a toolbox of solid-state reactions. *Chem. Mater.* 14:1455–71
106. Hayward MA. 2013. Soft chemistry synthesis of oxides. In *Comprehensive Inorganic Chemistry II*, ed. J Reedijk, KR Poepelmeier, pp. 417–53. Amsterdam: Elsevier
107. Ranmohotti KGS, Josepha E, Choi J, Zhang JX, Wiley JB. 2011. Topochemical manipulation of perovskites: low-temperature reaction strategies for directing structure and properties. *Adv. Mater.* 23:442–60
108. Gopalakrishnan J, Bhat V, Raveau B. 1987.  $A^I\text{LaNb}_2\text{O}_7$ : a new series of layered perovskites exhibiting ion-exchange and intercalation behavior. *Mater. Res. Bull.* 22:413–17
109. Toda K, Sato M. 1996. Synthesis and structure determination of new layered perovskite compounds,  $\text{ALaTa}_2\text{O}_7$  and  $\text{ACa}_2\text{Ta}_3\text{O}_{10}$  ( $A = \text{Rb, Li}$ ). *J. Mater. Chem.* 6:1067–71
110. Josepha EA, Farooq S, Mitchell CM, Wiley JB. 2014. Synthesis and thermal stability studies of a series of metastable Dion–Jacobson double-layered neodymium–niobate perovskites. *J. Solid State Chem.* 216:85–90
111. Kodenkandath TA, Kumbhar AS, Zhou WL, Wiley JB. 2001. Construction of copper halide networks within layered perovskites. Syntheses and characterization of new low-temperature copper oxyhalides. *Inorg. Chem.* 48:710–14
112. Kodenkandath TA, Lalena JN, Zhou WLL, Carpenter EE, Abd S, et al. 1999. Assembly of metal-anion arrays within a perovskite host. Low-temperature synthesis of new layered copper-oxyhalides,  $(\text{CuX})\text{LaNb}_2\text{O}_7$ ,  $X = \text{Cl, Br}$ . *J. Am. Chem. Soc.* 121:10743–46
113. Ranmohotti KGS, Montasseradi MD, Choi J, Yao Y, Mohanty D, et al. 2012. Room temperature oxidative intercalation with chalcogen hydrides: two-step method for the formation of alkali-metal chalcogenide arrays within layered perovskites. *Mater. Res. Bull.* 47:1289–94
114. Suzuki H, Notsu K, Takeda Y, Sugimoto W, Sugahara Y. 2003. Reactions of alkoxy derivatives of a layered perovskite with alcohols: substitution reactions on the interlayer surface of a layered perovskite. *Chem. Mater.* 15:636–41

115. Takeda Y, Momma T, Osaka T, Kuroda K, Sugahara Y. 2008. Organic derivatives of the layered perovskite  $\text{HLaNb}_2\text{O}_7 \cdot x\text{H}_2\text{O}$  with polyether chains on the interlayer surface: characterization, intercalation of  $\text{LiClO}_4$ , and ionic conductivity. *J. Mater. Chem.* 18:3581–87
116. Takeda Y, Suzuki H, Notsu K, Sugimoto W, Sugahara Y. 2006. Preparation of a novel organic derivative of the layered perovskite bearing  $\text{HLaNb}_2\text{O}_7 \cdot n\text{H}_2\text{O}$  interlayer surface trifluoroacetate groups. *Mater. Res. Bull.* 41:834–41
117. Petralanda U, Etxebarria I. 2015. Structural instabilities and sequence of phase transitions in  $\text{SrBi}_2\text{Nb}_2\text{O}_9$  and  $\text{SrBi}_2\text{Ta}_2\text{O}_9$  from first principles and Monte Carlo simulations. *Phys. Rev. B* 91:184106
118. Deleted in proof
119. Schaak RE, Mallouk TE. 2000. Topochemical synthesis of three-dimensional perovskites from lamellar precursors. *J. Am. Chem. Soc.* 122:2798–803
120. Cushing BL, Falster AU, Simmons WB, Wiley JB. 1996. A multivalent ion exchange route to lamellar calcium cobalt oxides,  $\text{Ca}_x\text{CoO}_2$  ( $x \leq 0.5$ ). *Chem. Commun.* 1996:2635–36
121. Cushing BL, Wiley JB. 1998. Topotactic routes to layered calcium cobalt oxides. *J. Solid State Chem.* 141:385–91
122. Hyeon KA, Byeon SH. 1999. Synthesis and structure of new layered oxides,  $\text{M}^{\text{II}}\text{La}_2\text{Ti}_3\text{O}_{10}$  ( $\text{M} = \text{Co}, \text{Cu}, \text{and Zn}$ ). *Chem. Mater.* 11:352–57
123. Amano Patino M, Smith T, Zhang W, Halasyamani PS, Hayward MA. 2014. Cation exchange in a 3D perovskite—synthesis of  $\text{Ni}_{0.5}\text{TaO}_3$ . *Inorg. Chem.* 53:8020–24
124. Ling CD, Argyriou DN, Wu GQ, Neumeier JJ. 2000. Neutron diffraction study of  $\text{La}_2\text{Ni}_2\text{O}_7$ : structural relationships among  $n = 1, 2,$  and  $3$  phases  $\text{La}_{n+1}\text{Ni}_n\text{O}_{3n+1}$ . *J. Solid State Chem.* 152:517–25
125. Zhang R, Senn MS, Hayward MA. 2016. Directed lifting of inversion symmetry in Ruddlesden-Popper oxide-fluorides: toward ferroelectric and multiferroic behavior. *Chem. Mater.* 28:8399–406
126. Cascos VA, Roberts-Watts J, Skingle C, Levin I, Zhang WG, et al. 2020. Tuning between proper and hybrid-improper mechanisms for polar behavior in  $\text{CsLn}_2\text{Ti}_2\text{NbO}_{10}$  Dion-Jacobson phases. *Chem. Mater.* 32:8700–12
127. Li W, Wang ZM, Deschler F, Gao S, Friend RH, Cheetham AK. 2017. Chemically diverse and multifunctional hybrid organic–inorganic perovskites. *Nat. Rev. Mater.* 2:16099
128. Lee MM, Teuscher J, Miyasaka T, Murakami TN, Snaith HJ. 2012. Efficient hybrid solar cells based on meso-superstructured organometal halide perovskites. *Science* 338:643–47
129. Weber D. 1978.  $\text{CH}_3\text{NH}_3\text{PbX}_3$ , a Pb(II)-system with cubic perovskite structure. *Z. Naturforschung B* 33:1443–45
130. Weber D. 1978.  $\text{CH}_3\text{NH}_3\text{SnBr}_x\text{I}_{3-x}$  ( $x = 0-3$ ), Sn(II)-system with cubic perovskite structure. *Z. Naturforschung B* 33:862–65
131. Jain P, nad Toby BH D, Kroto HW, Cheetham AK. 2008. Order–disorder antiferroelectric phase transition in a hybrid inorganic-organic framework with the perovskite architecture. *J. Am. Chem. Soc.* 130:10450
132. Sletten E, Jensen LH. 1973. Crystal-structure of dimethylammonium copper(II) formate,  $\text{NH}_2(\text{CH}_3)_2\text{Cu}(\text{OOCH})_3$ . *Acta Crystallogr.* B29:1752–56
133. Buser HJ, Schwarzenbach D, Petter W, Ludi A. 1977. Crystal-structure of Prussian Blue:  $\text{Fe}_4[\text{Fe}(\text{CN})_6]_3 \cdot x\text{H}_2\text{O}$ . *Inorg. Chem.* 16:2704–10
134. Xu WJ, Chen SL, Hu ZT, Lin RB, Su YJ, et al. 2016. The cation-dependent structural phase transition and dielectric response in a family of cyano-bridged perovskite-like coordination polymers. *Dalton Trans.* 45:4224–29
135. Thiele G, Messer D. 1980. S-thiocyanato and N-isothiocyanato linkage isomerism in the crystal-structures of  $\text{RbCd}(\text{SCN})_3$  and  $\text{CsCd}(\text{SCN})_3$ . *Z. Anorg. Allg. Chem.* 464:255–67
136. Xie KP, Xu WJ, He CT, Huang B, Du ZY, et al. 2016. Order–disorder phase transition in the first thiocyanate-bridged double perovskite-type coordination polymer:  $(\text{NH}_4)_2\text{NiCd}(\text{SCN})_6$ . *CrystEngComm* 18:4495–98
137. Du ZY, Zhao YP, He CT, Wang BY, Xue W, et al. 2014. Structural transition in the perovskite-like bimetallic azido coordination polymers:  $(\text{NMe}_4)_2\text{B}'\text{B}''(\text{N}_3)_6$  ( $\text{B}' = \text{Cr}^{3+}, \text{Fe}^{3+}$ ;  $\text{B}'' = \text{Na}^+, \text{K}^+$ ). *Cryst. Growth Des.* 14:3903–9

138. Zhao XH, Huang XC, Zhang SL, Shao D, Wei HY, Wang XY. 2013. Cation-dependent magnetic ordering and room-temperature bistability in azido-bridged perovskite-type compounds. *J. Am. Chem. Soc.* 135:16006–9
139. Bostrom HLB, Goodwin AL. 2021. Hybrid perovskites, metal-organic frameworks, and beyond: unconventional degrees of freedom in molecular frameworks. *Acc. Chem. Res.* 54:1288–97
140. Bostrom HLB, Senn MS, Goodwin AL. 2018. Recipes for improper ferroelectricity in molecular perovskites. *Nat. Commun.* 9:2380